Adhesion, atomic structure, and bonding at the Al(111)/α-Al_2O_3(0001) interface: A first principles study

Donald J. Siegel*,†
Department of Physics, University of Illinois at Urbana-Champaign, 1110 West Green Street, Urbana, Illinois 61801

Louis G. Hector, Jr.††
Surface Science Division, ALCOA Technical Center, ALCOA Center, Pennsylvania 15069-0001

James B. Adams§
Chemical and Materials Engineering Department, Arizona State University, Tempe, Arizona 85287-6006
(Received 5 February 2001; revised manuscript received 30 October 2001; published 8 February 2002)

We have performed a series of *ab initio* calculations to determine the atomic structure, ideal work of adhesion (W_{ad}), and bonding character of the Al(111)/α-Al_2O_3(0001) interface. Six candidate interface geometries were considered, including Al and O terminations of the oxide. Minimization of the Hellman-Feynman forces resulted in substantial changes to the atomic structure of the metal near the interface, wherein some atoms adopted positions consistent with a continuation of the oxide's Al-sublattice crystal structure across the interface. Consequently, the lowest-energy structures (i.e., having the largest W_{ad}) are those that facilitate this ''oxide extension'' mechanism. By applying several methods of analysis we have thoroughly characterized the electronic structure and have determined that Al-O bonds constitute the primary interfacial bonding interaction. These bonds are very similar to the cation-anion bonds found in the oxide bulk and are mainly ionic, yet maintain a small amount of covalent character. In addition, there is evidence of metal-cation bonding at the optimal Al-terminated interface. Taking into account recent theoretical and experimental evidence suggesting an Al termination of the clean oxide surface, our calculations predict $W_{ad}=1.36$ J/m^2 [local density approximation (LDA)] and 1.06 J/m^2 [generalized gradient approximation (GGA)] for the optimal Al-terminated structure, which are in good agreement with the experimental value of 1.13 J/m^2 as scaled to 0 K. These values are approximately an order of magnitude smaller than what is found for the optimal O-terminated interface: 10.70 J/m^2 (LDA) and 9.73 J/m^2 (GGA). Although cleavage preferentially occurs at the interface for the Al termination, strong bonding at the O-terminated interface favors cleavage within the metal.

DOI: 10.1103/PhysRevB.65.085415 PACS number(s): 68.35.−p, 73.20.−r, 71.15.Mb, 71.15.Nc

I. INTRODUCTION

Interfaces between metals and ceramics play a vital role in an increasingly large number of industrial applications: heterogeneous catalysis, microelectronics, thermal barriers, corrosion protection, and metals processing are but a few representative examples. Indeed, a large body of fundamental and applied research extending back nearly half a century has been devoted to understanding and optimizing the mechanical, electrical, and chemical properties of these interfaces.[1–5] However, experimental complications associated with the study of a buried interface and theoretical difficulties arising from complex interfacial bonding interactions have hindered the development of general, analytic models capable of accurately predicting fundamental interfacial quantities.

One such quantity, which is key to predicting the mechanical properties of an interface, is the ideal work of adhesion, W_{ad},[5] which is defined as the energy needed (per unit area) to reversibly separate an interface into two free surfaces, neglecting plastic and diffusional degrees of freedom. The energy needed in an actual cleavage experiment will always be greater than the ideal work of adhesion, due to plastic deformation, but the extent of plastic deformation is likely dependent upon W_{ad}. Formally, W_{ad} can be defined in terms of either the surface and interfacial energies (relative to the respective bulk materials) or by the difference in total energy between the interface and its isolated slabs:

$$W_{ad}=\sigma_{1v}+\sigma_{2v}-\sigma_{12}=(E_1^{tot}+E_2^{tot}-E_{12}^{tot})/A. \quad (1)$$

Here σ_{iv} is the surface energy of slab i, σ_{12} is the interface energy, E_i^{tot} is the total energy of slab i, and E_{12}^{tot} is the total energy of the interface system. A represents the *total* interface area.

To date, the available analytic models for predicting W_{ad} are limited to liquid-metal/oxide interfaces and rely on simple empirical correlations that incorporate either the free energy of formation of the oxide of the liquid metal or the enthalpies of mixing of the respective oxide elements in the metal.[1,2,6–10] Unfortunately, many of these models are not applicable to systems in which the ceramic is not an oxide, do not address solid-on-solid interfaces, can be difficult to parametrize, and generally provide only qualitative information about trends in adhesion. Furthermore, their range of applicability—even within the class of metal/oxide interfaces—is questionable, as many have only been applied to systems using α-Al_2O_3 (alumina) as the oxide.

In light of the shortcomings of the above models, it should come as no surprise that the last five years have seen

rapid growth in the number of first-principles studies of metal/ceramic adhesion based on density functional theory (DFT).[11,12] These methods are known to be very accurate and can provide valuable information regarding the detailed atomic and electronic structure of the interface.[5] Whereas most early studies focused on oxide ceramics and on a small number of model systems, there has recently been a move to study interfaces of more technological relevance,[13–22] while introducing more realistic models that incorporate interfacial defects and impurities,[23–25] more diverse geometries,[26] and environmental effects.[27]

One industrially relevant metal/ceramic interface is that between aluminum and its native oxide, Al_2O_3. Aluminum is one of the world's most widely used metals, in large part due to its superior strength-to-weight ratio, but also because of the favorable protective properties afforded by its oxide layer. This layer is predominantly amorphous,[28] with a thickness ranging from 3 to 6 nm, and consists of AlO_4 tetrahedra with a small number of AlO_6 octahedra.[29] The oxide can be created by direct oxidation of Al metal with O_2 at high temperatures—a process which proceeds rapidly and is highly exothermic.[30] Because of the difficulties associated with modeling an amorphous oxide/metal interface, for this study we have made a simplifying approximation by substituting the amorphous oxide with its thermodynamically stable phase, α-Al_2O_3. We believe this (admittedly) model system still embodies much of the essential physics of the true Al/Al_2O_3 interface. Despite its importance, there have been surprisingly few theoretical studies of this system, and we are aware of only one other *ab initio* calculation[31] which appeared during the preparation of this paper.

To our knowledge, the first theoretical study of atomic-scale adhesion at the Al/α-Al_2O_3 interface was performed by Anderson and co-workers.[32] They utilized a semiempirical molecular orbital method based on a cluster model to study cation vacancy diffusion in alumina and the adherence of alumina to Ni, Al, and Yt surfaces for one interface geometry. They reported an adhesion energy of 4.8 eV for the interface between a ten-atom Al cluster and an $[AlO_6]^{6-}$ cluster, and found that the presence of Yt at the interface at monolayer coverage greatly strengthened the bond between metal and oxide. Unfortunately, the influence of lattice relaxation was not examined; more recent studies[17,33] of metal adsorption and adhesion on alumina surfaces have shown these effects to be significant. Streitz and Mintmire[34,35] developed an electrostatic model (ES+) for alumina taking into account charge transfer between the cations and anions, and merged it with an embedded atom method (EAM) potential for metallic Al to study adhesion and adhesive failure at the Al/alumina interface. By equilibrating the interface at 100 K for 1–2 ps, they found that O atoms rapidly diffused into the Al, resulting in a relatively weak interface with a highly disordered interphase region. Subsequent application of a tensile stress to the system resulted in fracture under a maximum stress of 2 GPa with $\mathcal{W}_{ad} \simeq 0.3$ J/m^2. Angelo and Baskes[36] used the modified EAM to perform molecular dynamics simulations of the relative energetics of (111)-oriented Al islands on the basal plane of alumina. (The adhesion energy was not reported.) They found that the orientation with $[1\bar{1}0]_{Al}||[10\bar{1}0]_{Al_2O_3}$ gave the most stable structure, in good agreement with experiment,[37] and noted a significant increase in interlayer separation for the first two layers of the Al island relative to that of the bulk. It was suggested that this would weaken the interface, with fracture occurring within the metal.

Experimentally, two groups have reported heteroepitaxial growth of Al films on an α-Al_2O_3 substrate in ultrahigh vacuum (UHV).[37–39] At room temperature, Vermeersch and co-workers[38] found that for Al coverages of less than five monolayers, the Al film reacted with the alumina surface, giving rise to an Al suboxide layer with a $(\sqrt{31}\times\sqrt{31})R \pm 9°$ geometry. Further deposition resulted in clustering of the Al atoms followed by island growth. Deposition at 470 °C (Ref. 39) was characterized by the same suboxide formation for low coverages, followed by epitaxial growth with an orientation of $[\bar{2}11](111)_{Al}||\langle\bar{2}110\rangle(0001)_{Al_2O_3}$. In a more recent experiment, Medlin *et al.*[37] found three distinct grain orientations of the Al film relative to the substrate, with the primary orientation being $[\bar{1}10](111)_{Al}||[10\bar{1}0](0001)_{Al_2O_3}$ for growth at 200 °C. High-resolution transmission electron microscopy revealed an interface that was atomically sharp to within a few atomic layers, while atomic force microscopy of the surface morphology revealed large planar terraces characteristic of step-flow growth. We have adopted the orientation relationship of Medlin *et al.* in our calculations.

There have been many studies devoted to understanding the surface properties of α-Al_2O_3. These range from investigations of clean and hydrogenated surfaces[40–48] to the adsorption properties of metal overlayers,[33,49–53] water,[54–56] and organophosphorous acids.[57] Electrostatic considerations[58] as well as a number of experimental and theoretical studies suggest that the bulk crystal structure with a single terminating layer of Al yields the most stable *clean* (0001) surface. However, this issue is still a matter of debate, as Toofan and Watson[43] have reported a mixture of 2:1 O/Al-terminated surface domains using a tensor low-energy electron diffraction (LEED) analysis in UHV. A recent crystal truncation rod diffraction study[55] performed under ambient conditions has shown that the hydrated surface is O terminated with a semiordered layer of adsorbed water about 2.3 Å above the terminal oxygen layer. In practice, it has proved very difficult to create a clean surface due to the presence of hydrogen, even in UHV.[41,52] Therefore, one should be cautious in making direct comparisons between theoretical studies of clean surfaces/interfaces and experiments that may by H contaminated. As a first step towards simulating a more realistic fully hydrated interface, we have neglected the influence of hydrogen in this work and have focused instead only on clean surfaces and interfaces with either Al or O terminations. We have chosen to include O-terminated surfaces in our interfacial study in order to draw comparisons with the Al-terminated case and as a precursor to follow-up studies that will include the effects of adsorbed hydrogen and/or water. Furthermore, a recent study by Zhang and Smith[31] has shown that both interfacial terminations are pos-

sible, depending upon the partial pressure of O_2 gas. There is also experimental evidence that other alumina/metal interfaces, such as alumina/Nb, are O terminated.[59]

In addition to determining adhesion energies, the goal of this study is to systematically analyze the atomic and electronic structure of the Al/α-Al_2O_3 interface. Since quantities such as $\mathcal{W}_{ad}$ are intimately related to the interfacial atomic structure and bonding, an understanding of these issues is a prerequisite to formulation of a general theory of adhesion. First of all, in order to identify the energetically preferred structure, we have studied six candidate interface geometries, including two terminations of the oxide, and have allowed for full atomic relaxations. The optimal geometries are rationalized in terms of the bulk stacking sequence of the oxide. The second goal of this work is to illuminate the nature of the interface bonds through the application of several complementary analytical tools. This is necessary because the vastly different chemical environments within the constituent slabs make for a wide variety of possible interface bonds, ranging from highly delocalized (as in the Al) to highly ionic (as in the oxide). Unfortunately, no one method can completely classify the bonding, and we will demonstrate how the application of an ensemble of techniques is preferable. It will be shown that the ability of the metal to transfer charge to the oxide—and thereby form ionic bonds—is key to predicting the magnitude of $\mathcal{W}_{ad}$.

The remainder of this paper is organized as follows: Section II describes the background theory and computational methodology used in this study. Section III presents the results of our bulk and surface validation calculations on the pure materials. Section IV describes the six different interfacial geometries used in our simulations, and Sec. V outlines the methods used to calculate the lowest-energy structures and their corresponding adhesion energies. The results for the structure, adhesion, and bond character for the Al-terminated and O-terminated interfaces appear in Secs. VI and VII, respectively. Finally, we summarize our findings in Sec. VIII.

II. METHODOLOGY

For this study we utilized the Vienna *ab initio* Simulation Package (VASP),[60] which uses a plane-wave basis set for the expansion of the single-particle Kohn-Sham wave functions, and either ultrasoft or norm-conserving pseudopotentials[61,62] to describe the electron-ion core interaction. The ground-state charge density is calculated using a fast band-by-band residual minimization method—direct inversion of the iterative subspace algorithm[63,64] (RMM-DIIS) coupled with a Pulay-like mixing scheme.[63,65,66] Sampling of the irreducible wedge of the Brillouin zone is performed with a regular Monkhorst-Pack grid of special **k** points.[67] Due to numerical instabilities associated with integrating the step-function character of the 0-K Fermi-Dirac distribution, partial occupancies of the single-particle wave functions are introduced.[68,69] For calculations requiring accurate interatomic forces for supercells containing metallic Al, we have used the first-order method of Methfessel and Paxton[70] with an energy level broadening of 0.1 eV. Total energies were later calculated using the linear tetrahedron method with Blöchl corrections,[71,72] thereby eliminating any broadening-related uncertainly in the total energy. Ground-state atomic geometries were obtained by minimizing the Hellman-Feynman forces[73,74] using either a conjugate gradient[75] or quasi-Newton[63] algorithm. Finally, two separate approximations to the exchange-correlation energy were employed: the local density approximation (LDA) as parametrized by Perdew and Zunger[76] and the generalized gradient approximation (GGA) of Perdew *et al.*[77] (PW91).

Due to the substantial computational cost of performing a DFT calculation on a metal/oxide system, our molecular-static predictions of the structure and adhesion energies do not account for temperature and larger-scale size effects such as reconstructions.

III. BULK AND SURFACE CALCULATIONS

A. Bulk properties

We first verified the accuracy of the computational methods by calculating the bulk properties of Al and α-Al_2O_3. The Al calculations were performed using a norm-conserving Rappe-Rabe-Kaxiras-Joannopoulos-type[61] (RRKJ-type) pseudopotential in the separable Kleinman-Bylander[78] form. The *d* function was chosen as the local component, and the cutoff radius for matching of the all-electron and pseudo wave functions was set at 0.96 Å . Additionally, the nonlinear core-valence exchange-correlation interaction was accounted for by including partial core corrections. The total energy per atom was converged to within 1–2 meV upon using a plane-wave kinetic energy cutoff of 270 eV. The same degree of convergence in **k**-point sampling was attained using 110 **k** points in the irreducible Brillouin zone (IBZ).

The ground-state lattice constant a, bulk modulus B_0, and cohesive energy E_{coh} were determined via a fit of energy-volume data to the Murnaghan[79] equation of state. Both LDA and GGA functionals were considered. We find that the GGA does substantially improve the LDA overbinding errors in lattice constant [$a=3.971$ (4.039) Å, LDA (GGA); experiment: 4.03 Å (Ref. 80)] and cohesive energy [$E_{coh}=4.09$ (3.54) eV; experiment: 3.39 eV (Ref. 81)], yet it underestimates the bulk modulus with respect to experiment [$B_0=84.1$ (73.5) GPa; experiment: 79.4, 82.0 GPa (Refs. 82–84)]. In addition, our calculated values are in excellent agreement with other first-principles results.[85] However, since neither the GGA nor LDA gives superior agreement with experiment for all properties, we will use both throughout this work.

The crystal structure of alumina consists of a hexagonal close-packed array of oxygen atoms with Al atoms occupying two-thirds of the interstitial octahedral sites.[86,87] The structure can be viewed in either its primitive rhombohedral cell containing two molecular units (for a total of ten atoms), with $D^6_{3d}(R\bar{3}c)$ symmetry, or in the more traditional hexagonal unit cell containing six molecular units.

The bulk properties of alumina were calculated using a plane-wave cutoff energy of 400 eV and six **k** points in the IBZ. These values resulted in convergence in the total energy

TABLE I. Comparision of calculated α-Al_2O_3 bulk properties with experiment and a recent all-electron calculation (a and c denote the hexagonal lattice constants).

	a (Å)	c (Å)	B_0 (GPa)	E_{coh} (eV)
LDA	4.714	12.861	239	37.1
GGA	4.792	13.077	246	33.0
LDA[a]	4.767	12.969	244	36.5
Experiment	4.758[a]	13.00[a]	253[b]	31.8[c]

[a]Reference 87.
[b]Reference 89.
[c]Reference 90.

to within 1–2 meV per atom. We used the same norm-conserving pseudopotential for the Al atoms as used for bulk Al and an ultrasoft pseudopotential for O with an outer cutoff radius of 0.82Å .[88] The results of the Murnaghan fit for both LDA and GGA calculations are shown in Table I, and exhibit good agreement[85] with experiment and the all-electron first-principles calculations of Boettger.[87] As was the case for Al, our GGA calculations give slightly better agreement with the experimental data for the lattice constants and cohesive energy. An important point of validation is the good agreement with the all electron calculation.[87] This suggests that use of the pseudopotential approximation—often of questionable validity for highly ionic systems—is valid here.

B. Surface properties

Since a goal of this work is to simulate the structure, energetics, and bonding at a *bulklike* interface, it is essential that the interfaced slabs be thick enough to exhibit bulklike interiors. Otherwise one is simulating the adhesion properties of a thin film, which can be very different from that of the bulk. To ensure a bulklike interior we examined the convergence of the slab's surface energy with respect to slab thickness.

A second consideration is surface structure. It is well known that the Al-terminated (0001) surface of alumina undergoes an extensive relaxation that extends several layers into the bulk.[33] In order to predict accurate interface structures we performed an additional series of surface calculations to ensure that the relaxations of the first few atomic layers were converged with respect to slab thickness. Not surprisingly, we find that the convergence of the first few interlayer relaxations follows the convergence of the surface energy.

1. Al(111)

Experimentally, the Al(111) plane has been found to be the preferred interfacial plane for epitaxial growth of Al on α-Al_2O_3 (0001).[37,39] Additionally, since Al has the fcc crystal structure, the (111) surface is the most densely packed surface and therefore exhibits the lowest surface energy. Our Al(111) surface simulation cell has hexagonal geometry with one atom per layer, and the in-plane lattice vectors are consistent with the bulk lattice parameters as discussed in the preceding section (2.81 Å for LDA and 2.86 Å for GGA). In order to prevent unwanted interactions between the slab and its periodic images, a vacuum region must also be included in the cell; our convergence tests find that a 10 Å region is sufficient to converge the total energy of a five-layer slab to within 1–2 meV per atom. The same 1–2 meV degree of energy convergence with respect to **k**-point sampling was attained upon using 33 **k** points ($16\times16\times1$, Γ-centered grid) in the IBZ. All atomic positions in the slabs were optimized according to a conjugate gradient minimization of the Hellman-Feynman[73,74] forces until the magnitude of the force on each atom was 0.03 eV/Å or less.

TABLE II. Surface energy σ vs slab thickness for Al(111) and α-Al_2O_3(0001). Units are J/m^2.

System	No. layers	σ (LDA)	σ (GGA)
Al	3	0.97	0.76
	5	1.02	0.81
	7	1.02	0.81
	9	1.00	0.80
	11	1.02	0.82
α-Al_2O_3	9	2.02	1.50
	15	2.12	1.59
	21	2.12	1.59
	27	2.12	1.59

To determine the minimum thickness necessary for a bulklike Al slab, we have calculated the surface energy for slabs ranging from 3 up to 11 atomic layers (Table II) using the method proposed by Boettger and others.[91,92] We find that the surface energy is well converged by a five-layer-thick slab,[85] which is in good agreement with other studies of the effect of Al(111) substrate thickness on the adsorption energies of Na and K.[93]

We have also examined the relaxations of the Al(111) surface in order to ensure that they are reasonably converged as a function of slab thickness (Table III). Contrary to the large relaxations present in α-Al_2O_3(0001), the (111) surface of Al exhibits a small degree of interlayer relaxation, as one would expect of the close-packed face of an fcc metal. (The magnitudes of all relaxations are less than 2% of the bulk spacing.) Our calculations show that the sign of the first layer relaxation is only given correctly for slabs which are at least five atomic layers thick and is in good agreement with the other theoretical and experimental values. Although the sign of the second interlayer relaxation does not converge until slabs of seven layers are used, the absolute size of these relaxations is very small, on the order of 0.01 Å . Thus, given that the surface energy of the slab is converged at five layers and our belief that the increase in structural accuracy achieved by using a seven-layer slab is not justified by the accompanying increase in computational cost, we have used a five-layer Al slab for the remainder of our investigation.

2. α-Al_2O_3(0001)

Convergence tests on α-Al_2O_3(0001) showed that use of four **k** points in the IBZ and a vacuum region of 10 Å

TABLE III. LDA interlayer relaxations of the Al(111) surface as a function of slab thickness, given as a percentage of the bulk spacings.

	Theory							Experiment	
	Present (No. Layers)					Other			
Interlayer	3	5	7	9	11	Ref. 94	Ref. 95	Ref. 96	Ref. 97
1-2	−0.77	+1.92	+1.32	+0.61	+1.05	+1.18	+0.83	+0.9±0.5	+1.7±0.3
2-3		+0.42	−0.07	−0.46	−0.46	−0.40	−0.15		+0.5±0.7
3-4			−0.03	+0.11	+0.45	+0.22	+0.61		
4-5				−0.01	+0.25		+0.58		
5-6					−0.41				

yielded converged total energies to within 1–2 meV per atom. All atoms were relaxed to their ground-state positions by minimizing the magnitude of the Hellman-Feynman forces to a tolerance of 0.05 eV/Å /atom or less.

Table II gives the calculated LDA and GGA surface energies for alumina as a function of slab thickness for slabs ranging from 9 up to 27 atomic layers (corresponding to 3 and 9 molecular units, respectively). Once again we have used the method of Ref. 91 in order to avoid the problem of nonconvergence for thicker slabs. Very good convergence is attained upon using slabs which are 15 or more layers thick.[85]

Table IV lists our calculated LDA interlayer relaxations of Al-terminated α-Al_2O_3 (0001) surfaces of varying thickness for the first five interlayers.[98] As was the case for energy, we find that these relaxations are well converged for slabs containing 15 or more atomic layers and are in excellent agreement with the other first-principles results. The notable differences in magnitude and direction of relaxations predicted by theory with those from experiment are arguably caused by the presence of hydrogen and/or hydroxyl groups on the surface. For example, Hass and co-workers[54] showed that the presence of both molecular and dissociated water resulted in an outward movement of the terminating Al layer, thereby improving agreement with two recent experiments.[41,42] Wang and co-workers[48] have also shown that for an O-terminated surface the presence of hydrogen leads to an expansion of the terminal layer, in close agreement with experimental work reported by Toofan and Watson.[43]

In conclusion, we have shown that our calculated values of the bulk and surface properties for both Al and α-Al_2O_3 are in good agreement with available experimental and other first-principles results, thereby validating the application of this methodology to the study of interfacial properties.

IV. INTERFACE GEOMETRY

In general, there are an infinite number of ways two surfaces can be joined to form an interface: the surfaces can be created by cleaving along one of many possible planes, when dealing with compounds one has to choose amongst several surface stoichiometries, and finally there is a continuum of relative rotational and translational orientations. However, cystallographic considerations indicate that for an hcp crystal interfaced to an fcc crystal, the preferred orientation relationship is given by $(0001)_{hcp}||(111)_{fcc}$ and $[10\bar{1}0]_{hcp}||[\bar{1}10]_{fcc}$, in which the close-packed planes and directions are matched across the interface. This is the same orientation relationship found by Medlin *et al.*[37] for Al films grown epitaxially on a sapphire substrate (see also Ref. 39). Unfortunately, in that study it was possible to determine neither the chemical composition of the oxide's terminating layer nor the stacking sequence of the interfacial metal atoms relative to those of the oxide. In this work we have adopted the orientation relationship reported by Medlin *et al.* and have endeavored to determine the remaining unknown variables governing the structure of the interface. To these ends, we have considered three different stacking sequences and two different oxide terminations, for a total of six candidate interfacial geometries. The stacking sequences differ in the location of the oxide's interfacial O-layer with respect to the stacking sequence of the Al (111) surface and are illustrated in Fig. 1. Using the nomenclature of that figure: the "fcc" stacking

TABLE IV. LDA interlayer relaxations of the Al-terminated α-Al_2O_3(0001) surface as a function of slab thickness, given as a percentage of the bulk spacings.

		Theory									Experiment		
		Present (No. layers)				Other							
Interlayer		9	15	21	27	Ref. 48	Ref. 44	Ref. 33	Ref. 47	Ref. 54	Ref. 41	Ref. 42	Ref. 43
Al-O_3	1-2	−94	−83	−84	−83	−86	−86	−87	−85	−82	−63	−51	+30
O_3-Al	2-3	+2	+3	+3	+3	+6	+3	+3	+3	+7		+16	+6
Al-Al	3-4	−53	−46	−45	−46	−49	−54	−42	−45	−52		−29	−55
Al-O_3	4-5	+24	+19	+19	+19	+22	+25	+19	+20	+25		+20	
O_3-Al	5-6		+4	+4	+4	+6		+6					

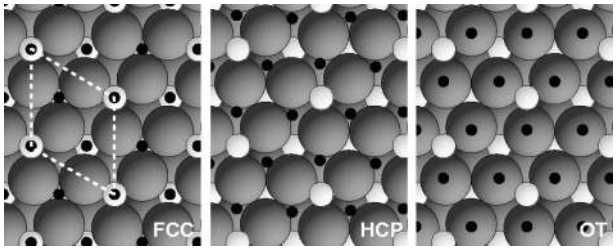

FIG. 1. Depiction of the three distinct interfacial stacking sequences. Large grey spheres represent O atoms, small white spheres represent Al atoms (also from the oxide slab), and black circles indicate the position of the interfacial layer of the Al(111) slab. The remaining four layers of the Al slab are omitted for clarity. The monikers ''FCC,'' ''HCP,'' and ''OT'' indicate the location of the oxide slab's interfacial oxygen layer with respect to the stacking sequence of the Al(111) surface. The dotted white parallelogram gives the outline of the simulation cell looking along the $[000\bar{1}]$ direction.

places the metal slab's interfacial atoms above the cation sites in the oxide, in the ''hcp'' stacking the metal atoms sit above the oxide's second O layer, and in the ''OT'' stacking the metal atoms sit directly above the surface O atoms. The oxide was chosen to be terminated by either a monolayer of Al or a monolayer of O. For each of these candidate geometries final interfacial structures were obtained by minimization of the Hellman-Feynman forces for all atomic coordinates.

Based on the results of our surface convergence tests, our model utilizes a 15-layer slab of α-Al_2O_3 (0001) arranged in a multilayer geometry between two 5-layer slabs of Al(111). There is a 10 Å vacuum region separating the free surfaces at the back of the Al slabs. This symmetric arrangement eliminates effects of spurious dipole interactions which might bias the results.[93] Each layer of the Al slab contains three atoms, and care has been taken to ensure that the two interfaces are identical. There are a total of 55 atoms in the supercells containing the Al-terminated interfaces and 53 atoms in the O-terminated models.

Based on differences in the in-plane lattice translation vectors of $(2a/3)[10\bar{1}0]_{Al_2O_3}=2.74$ Å and $a[\bar{1}10]_{Al}=2.86$ Å, the experiments presented in Ref. 37 calculated the lattice misfit of the interface to be 4.3%. The interface was observed to be semicoherent, in that the metal film was not found to be pseudomorphically strained through the film thickness to match the in-plane dimensions of the substrate. A misfit of this size suggests that close to the interface there are likely to be large regions of coherency—in which the metal film is strained to match the dimensions of the substrate—separated by a widely spaced periodic array of misfit dislocations. Since performing calculations on a supercell that accommodates the dislocation structure is impractical for a misfit of this size, our calculations use the coherent interface approximation, in which the softer Al slabs are strained to match the dimensions of the unreconstructed (1×1) α-Al_2O_3 (0001) surface unit cell. As our interface simulations use the bulk LDA lattice constants, the 3.1% misfit in our system is somewhat smaller than that which is found in experiment.[99] In practice, we are simulating the regions between dislocations. Even though our estimates of bond nature, atomic structure, and adhesion energy will be accurate for these regions, our estimate of the global adhesion energy will be approximate in the sense that it neglects misfit effects.[100]

V. COMPUTATIONAL PROCEDURE

We have used two methods to estimate the ideal work of adhesion, Eq. (1). The first method is based on the universal binding energy relation[101] (UBER), in which the unrelaxed slabs are brought incrementally closer together starting from a large initial separation and at each interface separation the total energy is calculated. The procedure continues until the energy passes through a minimum at the equilibrium separation and then begins to rise again for shorter distances. Finally, the energy versus distance data is fit to the UBER, yielding both the ideal work of adhesion and equilibrium separation as output.

The UBER has been successfully applied to interfaces constructed from slabs which do not exhibit significant surface relaxations and hence were well approximated by the truncated bulk material.[101–103] Unfortunately, this is not the case when dealing with α-Al_2O_3 (0001), and this leads to ambiguity in choosing the correct structure of the oxide surface: Is it best to use a relaxed or unrelaxed surface for the energy versus interfacial separation calculations or some combination of both? One could argue that using a bulklike termination is most realistic since the oxide will adopt a more bulklike structure when interfaced with Al. Yet this choice will yield the wrong structure at large separations since it neglects the energetically and structurally large relaxations of the oxide surface. One possible solution would be to use the UBER interfacial geometry as a starting point for an additional geometry optimization calculation. The work of adhesion could then be estimated by finding the energy difference between the *relaxed* interface and the *relaxed* isolated slabs. We have adopted this relaxation approach as our second method for calculating $\mathcal{W}_{ad}$ and will make comparisons with our (unrelaxed) UBER calculations below.

To minimize numerical errors, the calculations on each interface model were performed using the same **k**-point set and, where possible, the same supercell size. A thorough convergence test with respect to the number of irreducible **k** points was performed on the unrelaxed hcp Al-terminated interface geometry (hcp-Al) at an interfacial separation of 2 Å. It was determined that ten **k** points gave a converged $\mathcal{W}_{ad}$ to within about 0.03 J/m^2, and this set was then used for all subsequent calculations. Relaxed structures were generated using a combination of conjugate gradient and quasi-Newton minimization of the Hellman-Feynman forces. All atomic coordinates were optimized until the magnitude of the force/atom was less than 0.05 eV/Å.

Depending on the nature of the interfacial bonding and atomic structure, the *adhesive* bonds formed between the metal and ceramic may be stronger than the *cohesive* metallic bonds within the metal. To assess this possibility, we have

TABLE V. Relaxed and unrelaxed values for ideal work of adhesion (W_{ad}) and minimum interfacial distance (d_0). The units are J/m^2 and Å , respectively.

		Unrelaxed (UBER)		Relaxed		
Stacking	Termination	d_0	W_{ad} (LDA)	d_0	W_{ad} (LDA)	W_{ad} (GGA)
fcc	Al	2.55	1.14	0.70	1.36	1.06
hcp	Al	2.26	1.33	2.57	0.69	0.41
OT	Al	2.09	1.55	1.62	1.18	0.84
fcc	O	1.45	9.11	0.86	10.7	9.73
hcp	O	1.38	9.56	1.06	10.3	9.11
OT	O	1.71	9.43	2.00	9.90	8.75
	Experiment				1.13[a]	

[a]Reference 104.

performed a few additional calculations of W_{ad} at selected points within the metal, thereby simulating adhesive metal transfer to the oxide.

VI. ALUMINUM-TERMINATED INTERFACES

A. Adhesion and atomic structure

Results for UBER calculations on the Al-terminated interface systems are shown in Table V. A nonlinear least-squares fit to the *ab initio* LDA data gives the OT site as having the largest W_{ad} of 1.55 J/m^2, with the hcp and fcc sites ranking second and third, respectively. The values for the equilibrium interfacial separation are ordered such that the largest W_{ad} occurs for the smallest separation.

Taking the optimal structures given as output from the UBER calculations and using them as input for a series of LDA geometry optimization calculations yielded a different set of adhesion energies and interfacial separations. Table V compares these values to what was found for the UBER. As can be seen in the table, the relaxed values are of the same order of magnitude as those predicted by the UBER, but the *ordering* of the different sites has changed. Instead of the OT site having the strongest adhesion, the fcc site—which was predicted to have the weakest adhesion by the UBER calculation—is now preferred, with a drastically reduced interfacial separation of 0.70 Å , and $W_{ad} = 1.36$ J/m^2 (LDA), 1.06 J/m^2 (GGA). (An earlier study of Pt and Ag adsorption on alumina at a coverage of one monolayer also found the fcc stacking sequence to be perferred.[33]) These values are in good agreement with the experimental W_{ad} value of 1.13 J/m^2 (scaled to 0 K, as in Ref. 104) determined from the contact angle of a sessile drop of Al on a single-crystal substrate of alumina in vacuum.[105,106] The relaxed structure of this interface is shown in Fig. 2, where one can see that there are substantial changes in the atomic geometry of the Al slab atoms near the interface. The most notable feature is the large displacement of one of the metal atoms (labeled "Al_2") towards the oxide. This atom fills the cation site that would normally be occupied were the alumina crystal structure continued along the [0001] direction. It sits 1.46 Å above the O layer (O_1) in the alumina, which is close to the distance of 1.33 Å found in the bulk. (The "vacancy" in the Al created by the displacement of the Al_2 atom is too small —having a "nearest-neighbor" distance of about 1.7 Å —to accomodate a replacement Al atom via diffusion from the bulk.) The ability of the interface to realize this lowest-energy structure is facilitated by the fcc stacking sequence since it is the structure that initially places the Al slab above the octahedral holes in the alumina. In addition to this feature, there is also a noticeable buckling of the atomic positions within each layer of the Al well into the slab, and the center of mass of the entire slab has shifted slightly closer to the oxide. Finally,

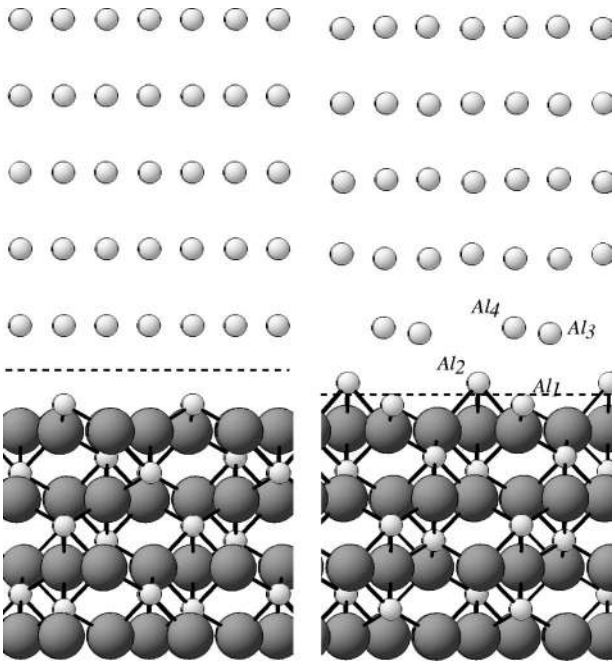

FIG. 2. Left: the lowest-energy geometry of the fcc-Al interface as predicted by UBER calculations. Right: the relaxed structure. Small spheres represent Al atoms; large spheres represent O atoms. The direction of view is along $[1\bar{2}10]$, and the location of the interface is indicated with a dashed line. The interfacial Al atoms are labeled according to their height above the interfacial O layer (O_1). The lower portion of the structure has been omitted.

the oxide's surface Al layer (Al_1) resumes a more bulklike position 0.76 Å above the O_1 layer upon formation of the interface, essentially undoing its relaxation in the clean surface. (This effect has also been seen for the adsorption of water and *d*-metal overlayers on alumina.[54,33]) In the bulk this distance would normally be 0.84 Å . The degree of atomic relaxation is much smaller in the other two stacking sequences.

We note in passing that the similarity of the magnitudes of $\mathcal{W}_{ad}$ as calculated by both methods is mainly due to a fortuitous cancellation effect between the relaxation energies of the interface and the isolated slabs. For many of the interfaces, the amount by which the energy of the interfacial structure is reduced by allowing for atomic relaxations is approximately equal to what is found for the slabs.

Upon completing the LDA calculations, we followed up with a series of "post-GGA" total energy calculations for each LDA geometry (Table V). We find that our PW91 GGA values for $\mathcal{W}_{ad}$ have the same trend, but are systematically smaller than the corresponding LDA results by about 20%–40%. Again, the fcc stacking sequence has the largest $\mathcal{W}_{ad}$ of 1.06 J/m^2, which is in better agreement with the experimental data than the LDA value. We note that this trend of predicting lower binding energies is consistent with what is generally seen for the GGA,[107] yet we feel that the nearly 40% deviation seen in the hcp stacking is unusually large. At present we have no explanation for this discrepancy, except to note that similar trends have been observed by others.[49]

B. Electronic structure and bonding

Apart from simply analyzing the atomic structure and energetics of these interfaces, we have used several methods to characterize the nature of the interfacial electronic structure and bonding.

1. Charge density

Figure 3 shows the planar-averaged valence charge density along a direction perpendicular to the fcc-Al interface for three different scenarios. In addition to showing the symmetry of the interface geometry, the figure also gives locations of the atoms by open and solid circles (Al and O atoms, respectively). The location of the interface is represented with a dotted vertical line.

The top panel of the figure gives the total charge density for the relaxed fcc-Al interface. When compared to the density from the unrelaxed (UBER) system in the middle panel, one can see that the Al slab atoms near the interface are displaced towards the oxide, with one of these atoms (Al_2) ultimately situated closer to the oxide than to the metal. As a result of this displacement there is a depletion of charge mainly within the first layer of the Al slab, indicative of weakened metallic bonding. This is a short-range effect, however, since the charge density returns to the bulk value by the second layer. Additionally, a small peak (identified by vertical arrows in Fig. 3) in the charge density appears between the Al_2 atom and the remaining interfacial metal atoms (Al_3, Al_4). As will be shown later, this can be explained in terms of covalent bonding, both within the metal

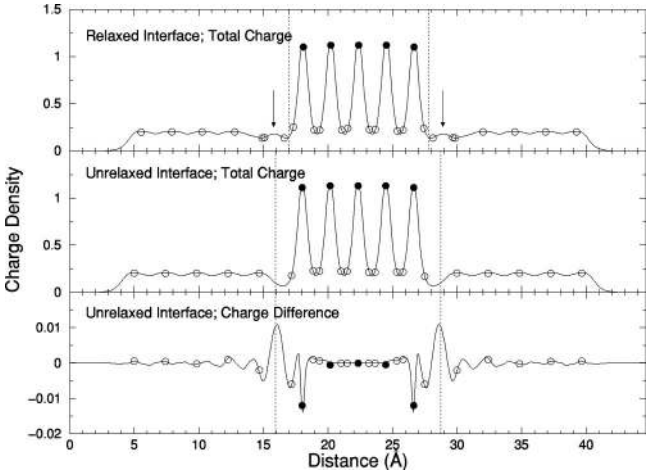

FIG. 3. Planar averaged total charge density for the fcc-Al interface along the (0001) direction. Solid circles give the location of the O atoms, open circles represent the Al atoms, and the vertical lines bisect the region separating the Al slab from the oxide slab. Top panel: charge density from the relaxed interface. Middle panel: charge density as predicted by the UBER calculation. Bottom panel: difference charge density (total UBER charge minus the charge density from the unrelaxed, isolated slabs).

(compensating for the reduction in metallic bonding) and *across* the metal/ceramic interface.

The middle and bottom panels of Fig. 3 show the total and difference charge density for the (unrelaxed) structure predicted by the UBER calculations. The difference charge was evaluated by subtracting the sum of the isolated slab charge densities from the total interface charge density. Unlike the charge profile for the relaxed interface, the unrelaxed charge shows virtually no distortion arising from interfacial bonding at any depth into the constituent slabs, yet there is a pronounced depletion region at the interface which is partially filled upon allowing for atomic relaxations. The difference charge density shows regions of charge depletion on the oxides's O_1 layer and Al_1 layers and on the first layer of the Al slab; there is relatively little change in the density for layers deeper into the slabs. The depleted charge accumulates in the interfacial region, suggesting a covalent bond. However, as we will later see, this interpretation is premature in that it neglects the important role played by atomic relaxations. Indeed, in allowing for atomic relaxations, a different picture of the bonding emerges, which contains elements of ionic bonding.

2. Partial density of states

Figures 4 and 5 show the layer-projected and Al-atom-projected densities of states (DOS), respectively, for the relaxed fcc-Al interface.[108] Looking at Fig. 4, we note first that the effect of the interface is rapidly screened by the metal slab, as there is little indication of changes to the bulk Al DOS beyond the interfacial layer. At the interface layer there is a small degree of overlap between the hybridized $3sp$ states on the Al atoms in the -17 to -14 eV range with the O $2s$ levels, suggesting a covalent, σ-type bonding. The effect of the interface on the oxide's DOS is also well local-

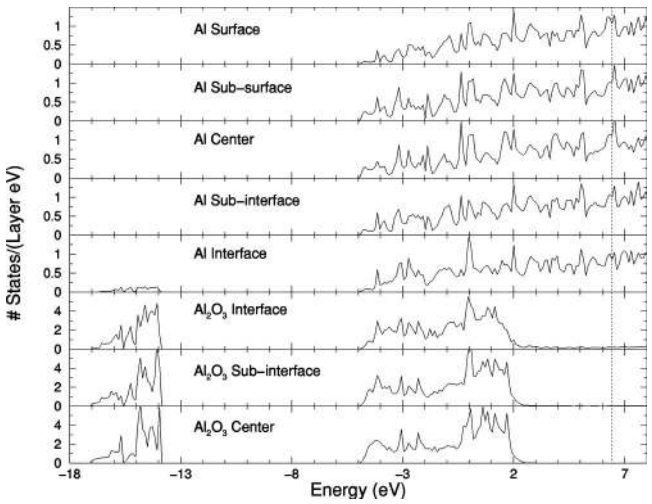

FIG. 4. Total DOS projected onto selected atomic layers for the fcc-Al interface. The projection begins in the top panel with the surface layer on the Al slab and progresses through this slab to the interface and finally into the center of the oxide. The dotted vertical line gives the location of the Fermi energy.

ized. (In the oxide a layer is defined as consisting of one molecular unit of alumina.) Apart from the presence of some metal-induced gap states (MIGS's) on the interface layer, the electronic structure is already bulklike by the subinterface molecular unit.

A more insightful way to visualize local changes to the electronic structure is to project the DOS onto selected Al atoms. This provides a common basis for comparison since Al is present in both slabs. It is then possible to single out individual atoms for analysis and thereby assess their importance in bonding without the ambiguity that results when DOS data are projected onto layers.

Looking then at Fig. 5 we notice several important features that are either not apparent or obscured in Fig. 4. First,

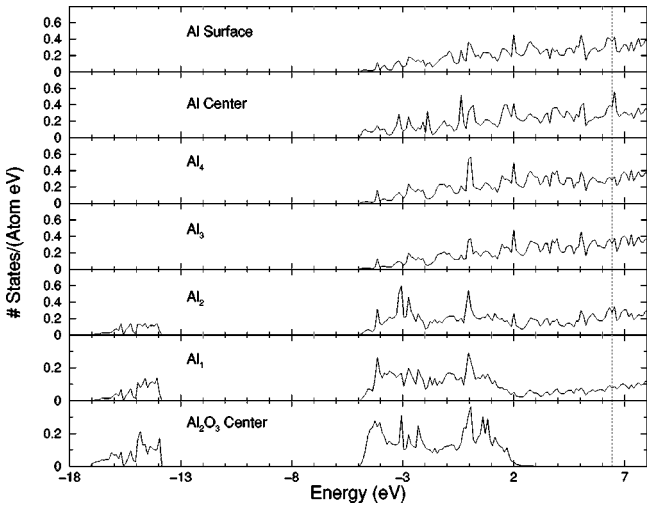

FIG. 5. Total DOS projected onto selected Al atoms for the FCC-Al interface. "Al_{1-4}" refers to the distinct interfacial Al atoms identified in Fig. 2. The vertical dotted line gives the location of the Fermi energy.

the aforementioned low-energy states on the interfacial Al layer are due to a bonding interaction involving *only* the Al_2 atom. This is the atom pulled towards the oxide and which ultimately occupies what would otherwise be a cation site in bulk alumina. In addition to the appearance of these new states, there is a depletion of states in the 2–6 eV range relative to the DOS for the more bulklike Al slab atoms. This is consistent with what is seen for the cations of the oxide (the Al_1 and "center" atoms), where the DOS in this range are either depleted or suppressed as they fall within the oxide's band gap. Finally, the Al_1 panel reveals that the MIGS's mentioned in the layer-projected DOS are to a large extent localized on the oxide's interfacial cation.

To summarize our findings from the DOS analysis, we see that the changes in electronic structure for both slabs are generally confined to regions close to the interface and that covalent bonding effects primarily involve only one atom from the metal slab (Al_2). The bond character is qualitatively similar to what is seen for the cation-anion interaction in the bulk oxide, involving overlap between hybidized Al $3sp$ states and O $2s$ states.

3. Electron localization

Although a DOS analysis can reveal valuable information about the nature of covalent bonding, it provides limited insight into matters related to ionicity and charge transfer. Recently, a novel graphical means for analyzing electron localization has been proposed and applied to the study of atoms, molecules, and solids.[109–112] The so-called "electron localization function" (ELF) allows one to identify regions of space having a high concentration of paired and unpaired electrons which can subsequently be interpreted as bonds, lone pairs, and dangling bonds. Depending on the topology and magnitude of the ELF it is also possible to distinguish between metallic, covalent, and ionic bonding types.

Figure 6 shows contour plots of the ELF data through two slices of the fcc-Al interface along the $(10\bar{1}0)$ and $(11\bar{2}0)$ planes. For clarity only one of the Al slabs (top) and slightly more than four O layers of the alumina slab (bottom) are shown; a portion of the vacuum region is also visible at the top of the slices. We have chosen the origin of the $(10\bar{1}0)$ plane so that the slice passes through both the Al_2 atom (which is closest to the alumina) and one of its nearest neighbor O_1 atoms, allowing one to see the bonding interaction between them. This slice also passes through several other Al-O bonding pairs deeper into the oxide and bisects many of the atoms in the Al slab. The $(11\bar{2}0)$ plane has its origin set so that it passes through all four Al atoms (Al_1–Al_4) adjacent to the O_1 layer. This positioning allows us to assess backbonding in the Al slab and any additional interactions between the Al slab and the oxide's Al_1-layer.

The magnitude of the ELF in the figure is given by a gray-scale color coding in which low values are represented by black, intermediate values by increasingly lighter shades of gray, and high values by white. By definition, ELF values fall within the interval $[0,1]$, and in our plots five equally spaced contour levels divide the range $[0,0.85]$. The ELF is approximately one both in regions where electrons are paired

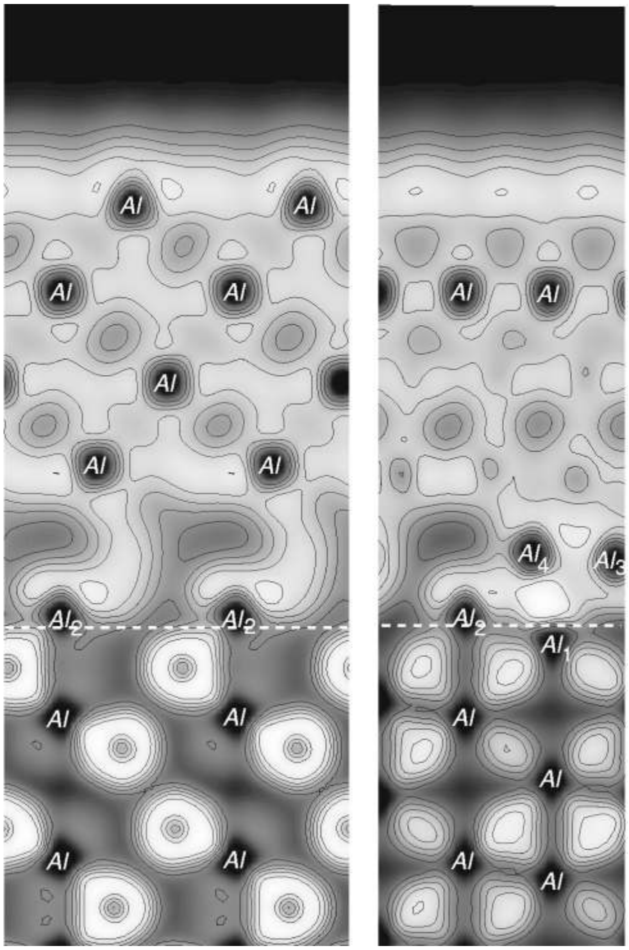

FIG. 6. Two slices through the ELF for the fcc-Al interface taken along the $(10\bar{1}0)$ (left panel) and $(11\bar{2}0)$ (right panel) planes, showing four of the hcp O layers in the oxide (bottom) and all five atomic layers from one of the Al slabs (top). The position of the interface is indicated by the dashed horizontal line, and the Al atoms which intersect the contour plane are labeled.

in a covalent bond and near lone electrons from a dangling bond. Since we are using pseudopotentials to simulate the effect of the atomic nucleus and core electrons, there is no physical significance to the data within the core regions, and the ELF assumes a small value there due to the low charge density.

Turning our attention towards the $(10\bar{1}0)$ plane (left panel), we note first the stark difference in ELF behavior between the metal and oxide slabs. In the bulk metal there is no evidence of strongly localized electrons, and the ELF assumes values close to 0.5 throughout the interstitial regions, which is characteristic of the homogeneous electron gas and metallic bonding. For the most part, changes to this behavior as a result of forming the interface are restricted to the interfacial layer. In contrast, the oxide consists mainly of regions of low charge density with most electrons localized on the O atoms. This indicates a highly ionic type of bonding. Nevertheless, there is still a small degree of covalency present, as the regions of high ELF (ELF "attractors") around the O atoms are not spherically symmetric and exhibit lobes directed towards the neighboring Al atoms. [The asymmetry is best seen in the $(11\bar{2}0)$ slice.] This corroborates our findings of limited covalency in bulk alumina from our preceding DOS analysis.

The $(10\bar{1}0)$ slice clearly illustrates the nature of the bonding between the O_1 layer and the subsumed Al_2 atom (whose location coincides with the region of low ELF just above the interface line in Fig. 6). In comparing the shape of the ELF near the Al_2-O_1 bond with that of the Al-O bonds deeper into the oxide, we see that they are practically *identical*: most of the charge remains localized on the O_1 atoms, with distortions of the ELF attractor directed towards the Al_2 atom. This confirms our conclusions from the DOS analysis showing that the Al_2 atom has an electronic structure approaching that of the cations in bulk alumina, and suggests that a main contribution to Al-O interfacial bonding is of a mixed ionic-covalent type similar to what is seen in bulk alumina.

In addition to the Al_2-O_1 interfacial bonds, Fig. 6 gives evidence for Al-Al covalent bonding across the metal/ceramic interface. This can be seen in the $(11\bar{2}0)$ plane as the prominent white region between the Al_4 atom and the Al_1 layer. Additionally, there is another backbonding covalent-type ELF attractor between the Al_2 atom and a neighboring atom in the metal slab (Al_4), which is just barely visible in the $(10\bar{1}0)$ slice. These covalent bonds explain the small peak in the charge density seen in the top panel of Fig. 3 between the Al_2 atom and the Al_3/Al_4 atoms.

Finally, the ELF shows that atomic relaxation within the Al slab results in the formation of a charge depletion region in the vicinity of the original (unrelaxed) position of the Al_2 atom. (Note the region of low ELF above the Al_2 atom in Fig. 6.) This reduction in charge density was also visible in Fig. 3. The weakened metallic bonding within this region suggests a possible cleavage point for the interface. To test this hypothesis, we calculated $\mathcal{W}_{ad}$ for cleavage between the subsumed metal atom (Al_2) and the remainder of the metal slab. This is equivalent to a scenario in which the metal atom most strongly bound to the oxide is transferred to the oxide upon separation of the interface, i.e., adhesive metal transfer. Our calculations give 2.06 (LDA)/1.63 (GGA) J/m^2 for cleavage within the metal versus 1.36 (LDA)/1.06 (GGA) J/m^2 at the interface, suggesting that adhesive metal transfer for this interface is unlikely.

4. Mulliken population analysis

In order to provide a semiquantitative measure of charge transfer and ionicity we performed a Mulliken population analysis[113] using the SIESTA electronic structure code.[114,115] SIESTA uses pseudopotentials and a basis set of pseudoatomic orbitals for expansion of the valence electron wave functions. Our calculations utilized a "single ζ plus polarization" ($s+p+d$ orbitals) basis set to achieve a self-consistent charge density on the relaxed interface structures generated by the converged plane-wave calculations. For the purpose of making comparisons, we also performed calculations on the bulk crystals. All calculations were checked for convergence with respect to **k**-point sampling; however, we

TABLE VI. Bond orders and Mulliken charges for the optimal Al- and O-terminated interfaces compared with the bulk oxide and metal. The Al atoms are labeled as in Figs. 2 and 7, and O_1 refers to the interfacial O layer..

	fcc-Al	fcc-O	α-Al_2O_3	Al
Atom		Mulliken charges		
Al_1	+0.4	+0.4	+0.73	
Al_2	+0.3	+0.2		
Al_3	+0.1	−0.05		
Al_4	−0.1	+0.1		
O_1	−0.47	−0.46	−0.49	
Bond		Bond order		
Al_1-O_1 (short)	0.7	0.65	0.67	
Al_2-O_1 (long)	0.42	0.45	0.5	
Al_1-Al_2	0.15	0.21		
Al_1-Al_3	0.24	0.19		0.26,[a] 0.30[b]
Al_1-Al_4	0.56	0.21		
Al_2-Al_3	0.03	0.45		
Al_2-Al_4	0.41	0.04		

[a](111) interplane.
[b](111) intraplane.

did not endeavor to check the basis set for completeness, as we are only interested in evaluating trends.

The first result made clear by our population analysis is that there is a net charge transfer from the metal slabs to the oxide. With this choice of basis, we find about 0.6 electrons (e) transferred from both Al slabs or about $0.3e$ per interface. (Since the absolute value of the Mulliken charges depends sensitively upon the choice of basis set, only differences between related structures using the same basis are meaningful in establishing trends.) By summing the charges layer by layer, we further find that most, if not all, of the charge lost by the metal comes only from the interfacial layer, as the remaining layers are each approximately neutral. Looking within this layer we find that it is the Al_2 atom that is mainly responsible for the charge transfer, with a charge of $+0.3e$ (see Table VI). It is interesting to note that in bulk alumina the corresponding Mulliken charge on the Al cations is $+0.73e$, which is slightly more than twice the value found for the Al_2 atom. This seems reasonable since this atom has only half the number of nearest-neighbor oxygens (3) it would have in bulk alumina (6). Furthermore, there are two different types of Al-O bonds in the bulk: three ''long'' bonds each of 1.97 Å and three ''short'' bonds of 1.86 Å , and one would expect that the anions closer to the cation would exert a relatively stronger oxidizing effect. Since the Al_2 atom sits in one of the long bond sites we expect it to be oxidized by less than half the amount it is in the bulk, consistent with our results. Additionally, the oxide's Al_1 layer (which has short bonds to the three O_1 atoms) has an effective charge of $+0.4e$, slightly more than half of what is found in the bulk.

The remaining two atoms in the metal interfacial layer (Al_3, Al_4) exhibit smaller charges which are equal in magnitude but opposite in sign: about +0.1 and −0.1 electrons, respectively. These two charges appear to be the result of an image interaction.[116–118] Even though all the interfacial metal atoms sit in hole sites above the O_1 layer, these sites are not identical (see Fig. 1): one is located directly above the alumina's interfacial cation, while the remaining two are adjacent to O atoms, but they differ in their distance to the cations deeper into the alumina. Consistent with image charge theory, both metal atoms neighboring the negatively charged O atoms assume positive charges of $+0.3e$ and $+0.1e$, respectively. Likewise, the Al_4 atom closest to the alumina's Al_1 layer (at $+0.4e$/atom) takes on a negative charge of $-0.1e$.

Excluding the Al_1 layer, the Mulliken population values for the remainder of the oxide atoms are nearly identical to what is found in the bulk. This is to be expected because in the fcc stacking sequence, the interfacial O atoms are still able to maintain their fourfold coordination by oxidizing the subsumed Al_2 atom. The formal charge on each O atom is approximately $-0.47e$, with each Al cation at $+0.73e$.

Our finding of charge transfer from metal to oxide differs from what was observed by Verdozzi *et al.*[33] in their DFT study of the bonding between Pt and Ag monolayers on Al-terminated α-Al_2O_3(0001). They reported bonding caused by metal polarization to the oxide's surface electrostatic field. On the other hand, a calculation (using a different local basis set) of bulk Nb on the same substrate by Batirev and co-workers[17] found a partially ionic metal-ceramic bond in which $0.37e$ were transferred to the oxide.

5. Bond order analysis

Just as a Mulliken population analysis can provide a semiquantitative measure of ionicity, a Mayer bond order analysis[119] can give insight into the relative strength of ionic and covalent/metallic bonding between a given pair of atoms. This is done by assigning a numerical value to the bond in question. In an ideal situation (i.e., for an ''appropriate'' choice of basis set) a vanishing bond order would indicate either no bonding or a perfectly ionic bond. A value of unity would correspond to a single covalent bond, a double bond would have a value of 2, etc. Fractional values would then be interpreted as a mixture of ionic and covalent bonding, or metallic bonding.

Batirev and co-workers[17] recently demonstrated the value of a bond order analysis in an interface study of Nb(111) on α-Al_2O_3(0001), in which they found hybridization between Nb $4d$ and O $2p$ levels for the Nb-O bonds formed at an O-terminated interface. These bonds were found to extend into the second layer of the Nb, with bond orders of 0.6 and 0.3, for the first and second layers, respectively. In this section we describe the results of our bond order analysis performed on the optimal relaxed fcc-Al interface. We have once again used the SIESTA code, which we modified to calculate this information.

We have calculated bond orders for four systems: the bulk aluminum crystal, the bulk oxide, and the fcc O- and Al-terminated interfaces. Table VI shows that in bulk alumina the bond order of a short Al-O bond is 0.67 when using the ''single ζ plus polarization'' basis. We find no significant deviations from this value for the same bonds within the oxide slab in the relaxed interface. Here the average short

bond order is about 0.66, and it is generally independent of proximity to the interface. One exception occurs, however, for the bonds between the oxide's Al_1 layer and its neighboring O_1 atoms. Here there is a slightly larger bond order of 0.7, suggesting a small increase in covalency with respect to bonds found in the bulk. The long Al-O bonds have a smaller bond order of 0.5, consistent with a reduction in covalency as a result of their longer bond length. These are also relatively insensitive to position within the slab.

Table VI also shows that the nearest-neighbor bond order in bulk Al is 0.26. This value is not maintained for all bonds in the interfacial Al slabs, as the lateral compression of the slabs (which was necessary to match the in-plane lattice constants of the metal to those of the oxide across the interface) induces an asymmetry in the bond orders between atoms within the same (111) plane versus those in adjacent planes. We find that in regions away from the interface the *intraplane* bond orders assume a value of 0.3, while the *interplane* bonds are identical to that found in the (unstrained) bulk, at 0.26. Presumably this agreement is a result of allowing for atomic relaxation in the [111] direction.

Unlike what was seen in the oxide, the presence of the interface generates changes in bond orders within the metal slab. These are confined to interactions either between the distorted interfacial layer and the next deepest layer (l_1-l_2 type) or within the interfacial layer itself (l_1-l_1 type). For l_1-l_2 bonding, we find that on average the bonds become more covalent, with a bond order of 0.35. The largest bond order within the metal, 0.41, occurs for the l_1-l_1 backbond between the Al_2 atom and one of its nearest neighbors, Al_4. Although the two atoms engaged in this bond were originally part of the same layer, the relaxation of the Al_2 atom towards the oxide has practically created a new layer closer to the interface. A portion of this bond can be seen in the $(10\bar{1}0)$ ELF slice of Fig. 6 as the white region to the upper right of the Al_2 atom. We conclude that formation of the interface results in a reduced metallic bonding within the near-interface regions of the metal in favor of forming more directional, covalent-type backbonds.

Obviously, the most important bonds in this system are those which span the interface. These can be divided into two groups. The first involves the three Al_2-O_1 bonds. In our earlier ELF and Mulliken analysis, we concluded that these bonds were qualitatively similar to the long Al-O bonds found in the bulk oxide. By comparing the bond orders at the interface with those found in the bulk we can determine *how* similar they are. Our calculations give: 0.38, 0.46, and 0.43, respectively, for the three bonds, for an average bond order of 0.42 (see Table VI). This is only slightly smaller than the corresponding bulk value of 0.5, thereby confirming our earlier analysis. The deviation can be explained by differences in the bond lengths. In the bulk, the normal bond length is 1.97 Å , whereas at the interface these three bonds are all longer, with lengths of 2.03, 2.11, and 2.04 Å , respectively. (The longer bonds have the smaller bond orders.) This signals a small reduction in covalency. We ultimately conclude that these bonds are similar to, yet somewhat weaker than, the long Al-O bonds found in bulk α-Al_2O_3.

The second type of interfacial bond links the oxide's Al_1 layer to an interfacial metal atom (Al_4) with a relatively large bond order of 0.56. This is about twice the value of other Al-Al bonds in the metal and is easily seen in the $(11\bar{2}0)$ slice of Fig. 6 as the large white region at the interface. This appears to be a covalent interaction, as evidenced by the compact shape of the ELF attractor. This is a somewhat surprising result, as we did not expect to find significant bonding between the oxide's cations and the metal. It would be interesting to determine what fraction of $\mathcal{W}_{ad}$ could be attributed to this bond and to compare the adhesion properties of our Al/α-Al_2O_3 system to those involving other corundumlike oxides with different cations: i.e., α-Fe_2O_3 and α-Cr_2O_3. Interfaces using these oxides will be the subject of a future study.

Finally, we note the presence of some weaker hybridization between the Al_1 layer and the Al_3 atom. The bond order here is 0.24, in close agreement with the metallic bond orders deeper into the Al slab. This interaction would account for the metal-induced gap states on the interfacial oxide layer seen in Fig. 4.

6. Summary of bonding analysis

We have found that there are two primary bonding interactions present at the fcc-Al interface. First, as revealed by the DOS, ELF, and bond order analyses, the Al-O bonds formed between the Al_2 atom and the alumina's O_1 atoms are similar to the long Al-O bonds found in the bulk oxide and are therefore mainly ionic with a smaller degree of covalency. Second, our bond order and ELF analyses showed that there is a covalent interaction between the oxide's Al_1 (surface cation) layer and the Al_4 atom from the interfacial metal layer. Additionally, the atomic displacements within the metal's interfacial layer create small charge depletion regions that disrupt the metallic bonding. To compensate, Al-Al covalent backbonds are formed, which make cleavage within the metal unfavorable with respect to cleavage at the interface. Finally, although there is charge transfer from the metal to the oxide, within the oxide there are only small deviations from bulklike bonding behavior, as the bond orders and Mulliken charges maintain their bulk values right up to the interfacial layer.

VII. O-TERMINATED INTERFACES

A. Adhesion and atomic structure

The properties for the O-terminated interfaces are very similar to those of the Al-terminated ones: they undergo a similar relaxation, have the same preferred stacking sequence, have similar features in the DOS, and exhibit many of the same types of bonding. The major difference, then, is one of magnitude. The adhesion, relaxation, and bonding are all significantly stronger for the O-terminations. This is to be expected considering that a major component of the bonding in the Al-terminated case was ionic. By removing the oxide's surface Al layer, the exposed O_1 layer becomes even more reactive (due to the presence of dangling O bonds), and it has

a correspondingly more pronounced effect on the atomic and electronic structure of the neighboring metal slab.

Table V shows the results of a UBER fit for the three stacking sequences of the O-terminated interfaces. Unlike the Al terminations—in which there were substantial differences in $\mathcal{W}_{ad}$ and d_0 between the different stackings—here the differences are minor, with all stackings having roughly $\mathcal{W}_{ad} \simeq 9$ J/m^2 and $d_0 \simeq 1.5$ Å. As a consequence of the strong Al-O interaction, the $\mathcal{W}_{ad}$ values are now nearly an order of magnitude larger, with the hcp stacking having the largest value, $\mathcal{W}_{ad} = 9.56$ J/m^2. Even the stacking with the largest interfacial separation is still more than 0.4 Å closer than the smallest separation found for the Al terminations.

Starting from the minimum energy UBER configurations, further geometry optimizations yielded the relaxed $\mathcal{W}_{ad}$ and d_0 values also listed in Table V. As was seen for the Al terminations, relaxation results in a *reordering* of the adhesion energies for the different stackings. Whereas the hcp stacking was preferred according to the UBER calculation, the fcc geometry has the largest $\mathcal{W}_{ad}$ after allowing for relaxation, with an increase of nearly 1.6 J/m^2 (LDA) over the unrelaxed result to a value of 10.7 J/m^2. We note that once again the system with the largest adhesion energy also has the smallest interfacial separation. This result is in partial agreement with Bogicevic and Jennison's[49] calculations for adsorption of Al on "ultrathin," O-terminated Al_2O_3 films. In contrast to our results, they found that at a coverage of 1 ML the OT site was preferred. However, for coverages greater than 1 ML, *either* the fcc or OT site was favorable. Finally, comparing the post-GGA adhesion energies with the corresponding LDA values, we find that the GGA predicts the same relative ordering of the adhesion energies, but with a slightly reduced magnitude of about 10%–15%.

Our values of $\mathcal{W}_{ad}$ for the Al/α-Al_2O_3 interface are less than those found for the Nb/α-Al_2O_3 system in Ref. 17. In particular, our GGA value of 1.06 J/m^2 for the fcc-Al geometry is less than half that found for the corresponding Al-terminated Nb/α-Al_2O_3 structure, 2.8 J/m^2. However, for the O-terminated systems our value is only slightly smaller: 9.73 J/m^2 vs 9.8 J/m^2. This trend is consistent with Bogicevic and Jennison's[49] calculations, in which for coverages up to 1 ML, Nb overlayers were found to bond more strongly than Al to an Al_2O_3 substrate.

Both the optimal UBER and relaxed geometries of the FCC stacking sequence are shown in Fig. 7. The presence of the interface induces large changes in the local atomic structure of the metal well into the subinterface layer. Instead of only one atom from the interfacial metal layer being pulled towards the oxide (as was the case for the Al termination), there are now *two* atoms which sit in the alumina's cation sites (Al_1, Al_2). The atom closest to the oxide (Al_1) rests 0.86 Å above the O_1 layer, a mere 0.02 Å farther than in bulk alumina, and has bond lengths of 1.87, 1.84, and 1.83 Å with its nearest-neighbor O_1 atoms, as compared to the bulk distance of 1.86 Å. The second displaced Al (Al_2) sits 1.42 Å above the O_1 layer, compared to the bulk spacing of 1.33 Å. It forms three long Al_2-O_1 bonds of length 1.96, 1.97, and 2.17 Å. The corresponding bond length in the bulk is 1.97 Å. These relaxations create a small void in the metal,

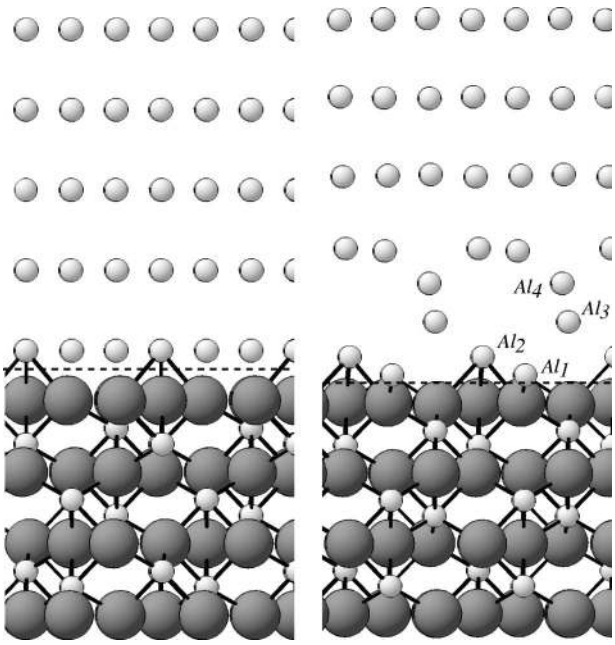

FIG. 7. Left: the lowest-energy geometry of the fcc-O interface as predicted by UBER calculations. Right: the relaxed structure. The direction of view is the same as in Fig. 2.

separating what remains of the Al slab from the newly extended oxide structure. There are no significant changes in the oxide structure. Additionally, a third metal atom (Al_3) in the subinterface layer relaxes towards the interface, and the center of mass of the entire Al slab shifts away from the oxide. The remaining two stacking sequences undergo substantially smaller relaxations.

An interesting consequence of allowing for atomic relaxations is the insensitivity of the oxide's final interfacial structure to its initial termination. By comparing the relaxed fcc structures of either termination (Figs. 2 and 7), we notice that in both cases the oxide is ultimately terminated by a *bilayer* of Al, with a geometry very similar to what is found in the bulk. In effect, the oxide has extended its stacking sequence across the interface in such a way that it seems more natural to consider the subsumed atoms as part of the alumina, with the true location of the interface shifted towards the metal.

B. Electronic structure and bonding

1. Charge density

Figure 8 shows the planar-averaged charge density for the fcc-O interface. Contrary to what was seen for the Al-terminated interface, the relaxed charge density is now depleted relative to the bulk in both the first *and* second layers of the Al slab, and is accompanied by a more substantial atomic rearrangement extending to the same depth. Within this charge depletion region there are two small peaks in the charge density (indicated by vertical arrows in Fig. 8), consistent with the formation of Al-Al covalent backbonds between the displaced Al atoms. The unrelaxed total density is relatively featureless except for the disappearance of the interfacial depletion region that was present in the fcc-Al sys-

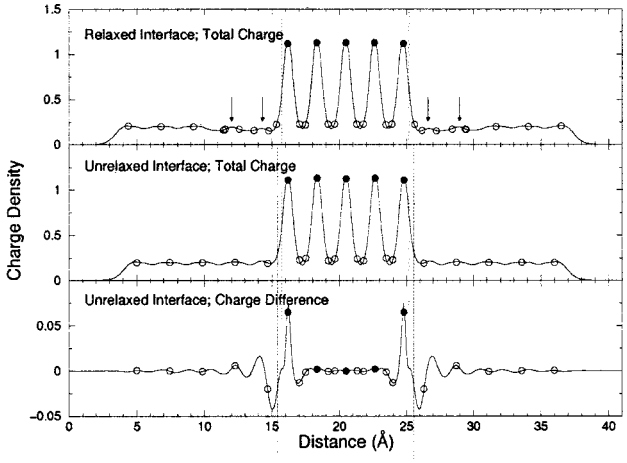

FIG. 8. Planar-averaged total charge density for the fcc-oxygen interface along the (0001) direction, using the same conventions as Fig. 3.

tem, Fig. 3. This is a result of the smaller interfacial separation in the O-terminated geometry. In the charge difference plot we note a depletion of charge around both Al atoms adjacent to the undercoordinated interfacial O atoms. Not surprisingly, this missing charge makes its way onto the more electronegative O ions, indicating the formation of an ionic bond, which will be verified by subsequent analyses of the electronic structure.

2. Partial density of states

The layer-projected (Fig. 9) and Al atom-projected (Fig. 10) DOS for the fcc-O interface share many features with that of the fcc-Al system: the effects of the interface on the electronic structure of both the metal and the oxide are localized to within the first layer, there is a metallization

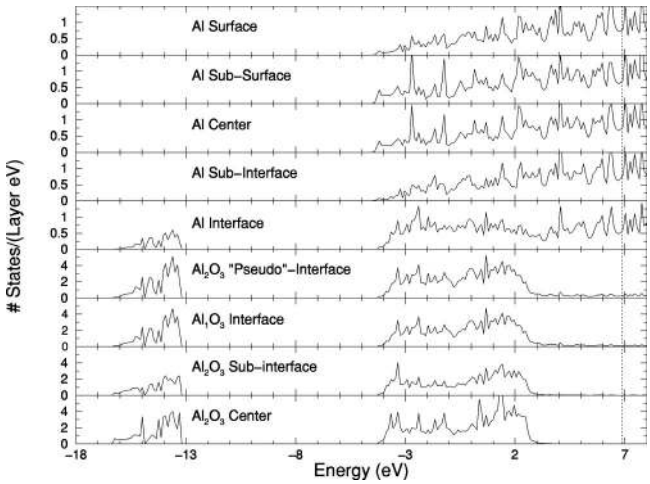

FIG. 9. Total DOS projected onto selected atomic layers for the fcc-oxygen system. The projection begins in the top panel with the surface layer on the Al slab and progresses through this slab to the interface and finally into the center of the oxide. The "Al_2O_3 pseudointerface" layer groups the Al_1O_3 interfacial unit from the oxide with the adjacent Al atom from the metal slab. The vertical dotted line gives the location of the Fermi energy.

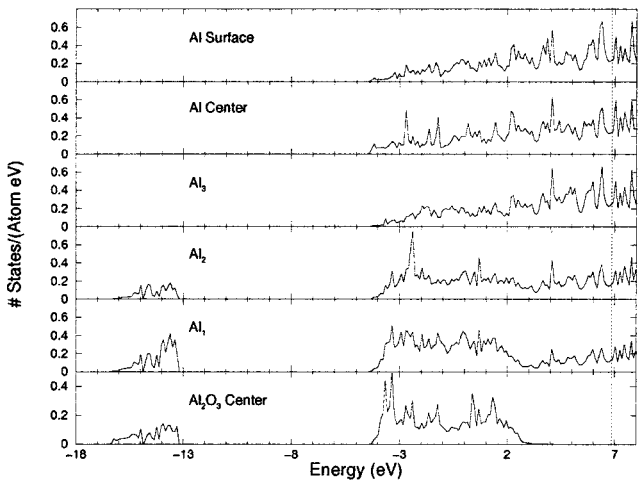

FIG. 10. Total DOS projected onto selected Al atoms for the fcc-oxygen system. "Al_{1-3}" refers to the three interfacial Al slab atoms identified in Fig. 7, and the vertical dotted line gives the location of the Fermi energy.

(MIGS's) of the interfacial oxide layer, and there is a set of new low-energy states present on the interfacial metal atoms in the -16 to -13 eV range due to overlap with the O_1 $2s$ states. The main difference between the O and Al terminations is that there are now *two* atoms from the Al slab that participate in bonding with the interfacial O_1 layer. These are the two atoms (identified as Al_1 and Al_2 in Fig. 10) that are pulled closest to the oxide and which sit in the cation sites (see Fig. 7). Both exhibit the appearance of new overlap states with the O_1 $2s$ levels, and both show a depletion of states in the energy range coinciding with the oxide's band gap. Yet it is the Al_1 atom (closest to the oxide) that experiences the most pronounced changes in electronic structure, as its DOS closely resembles that of an Al atom from the center of the oxide ("Al_2O_3 center"). Because two atoms now participate in covalent interactions with the oxide, the distortion of the Al slab's interfacial layer DOS (the "Al interface" in Fig. 9) is more substantial than in the Al-terminated case: there now appear to be roughly twice as many states overlapping with the O_1 $2s$ levels, and the depletion within the oxide's band gap is more pronounced. We therefore conclude that there is still some degree of covalency maintained in the interfacial bonds between the subsumed metal atoms and the O_1 layer. Furthermore, since the DOS projected onto these metal atoms is qualitatively similar to what is seen in the bulk oxide, it is reasonable to classify the Al-O_1 interface bonds as being similar to those found in bulk alumina.

3. Electron localization

Two contour plots of the ELF for the fcc interface are shown in Fig. 11, using the same orientation as in Fig. 6. As was seen for the Al-terminated fcc interface, the bonding interaction between the two subsumed metal atoms and the alumina's O_1 layer is remarkably similar to the Al-O interactions visible in the oxide bulk. The majority of the charge is located on the anions—but in a highly asymmetric

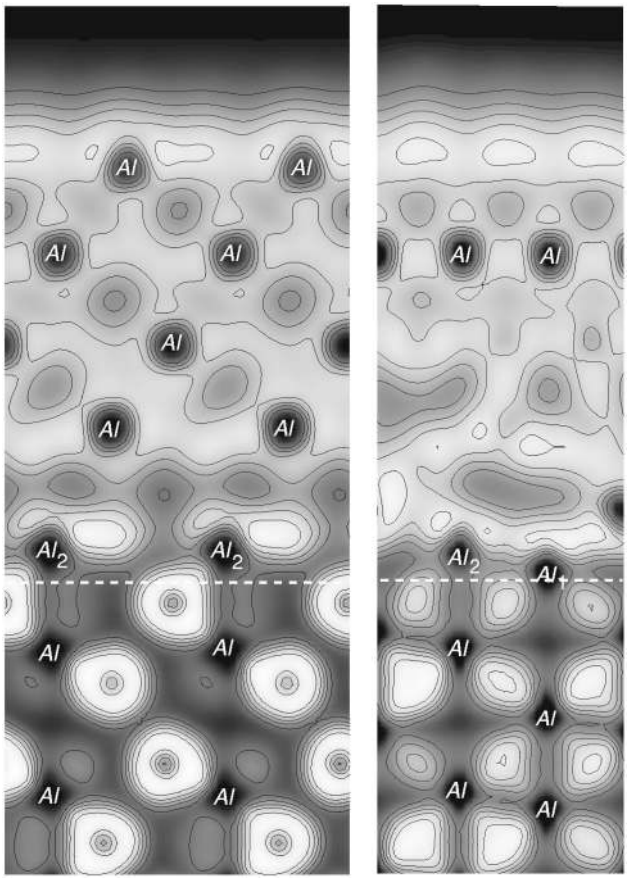

FIG. 11. Two slices through the ELF for the fcc-oxygen interface taken along the $(10\bar{1}0)$ (left panel) and $(11\bar{2}0)$ (right panel) planes.

fashion—with lobes directed towards their neighboring cations. We thus conclude that the bonding is again mainly ionic with a smaller degree of covalency. In further likeness to the Al-terminated interface, we also find regions of increased charge localization just above the interface in the $(10\bar{1}0)$ slice. These indicate the formation of covalent backbonds between the subsumed metal atoms and the remainder of the Al slab, which compensate for the disruption in metallic bonding induced by the large changes in atomic geometry and ionic bonding. The atomic rearrangements are also responsible for the creation of a series of small voids in the charge density that extend well into the second layer of the Al slab, as seen in the $(11\bar{2}0)$ slice. In comparison, the voids are localized to within the first metal layer in the fcc-Al interface, Fig. 6. These regions of low density suggest a weakening of the structural integrity of the Al slab and indicate a likely failure point for the interface under tensile stress applied perpendicular to the interface. Indeed, by cleaving the interface within the metal (between the Al_1 and Al_2 layers), we calculate $\mathcal{W}_{ad} = 0.67/0.56$ J/m^2 (LDA)/(GGA), which is more than an order of magnitude smaller than the 10.7/9.73 J/m^2 (LDA)/(GGA) required to break the bonds at the original location of the metal/ceramic interface. A similar case of adhesive metal transfer was observed by Batirev and co-workers[17] in their study of the O-terminated Nb/α-Al_2O_3 interface. They found that it was more favorable to cleave Nb-Nb bonds, and thereby transfer 1 ML of Nb to the oxide, than to cleave the strong Nb-O bonds at the interface.

4. Mulliken population analysis

Not surprisingly, a Mulliken analysis for the fcc-O interface reveals a much larger ionic interaction than was present in the fcc-Al system. There is now more than *double* the amount of charge transferred from the metal slabs to the oxide, about $1.3e$ total, or about $0.65e$ per interface. Whereas in the fcc-Al geometry most of this charge came from the one subsumed metal atom, now at least three metal atoms are found to participate in ionic bonding, with charge depletion present into the second interfacial metal layer (see Table VI). The two metal atoms closest to the oxide have charges of $+0.4e$ (Al_1) and $+0.2e$ (Al_2), with a smaller charge of $+0.1e$ found on one atom (Al_4) in the next deeper layer of the metal. The third interfacial metal atom (Al_3) has a slight negative charge of $-0.05e$. We note that the charge on the closest subsumed atom is *identical* to that found on the oxide's interfacial Al_1 layer in the fcc-Al case ($+0.4e$). This is to be expected since these atoms occupy essentially the same position. The Al_2 atom has a smaller charge of $+0.2e$ relative to the same in the fcc-Al structure ($+0.3e$). This reduction can be partially explained by charge depletion further into the metal slab, since by adding the charge on this atom to that of its Al_3 and Al_4 neighbors ($0.2e+0.1e-0.5e$) we recover most of the charge found in the Al-terminated structure. As before, the charges on the oxide atoms show little indication of disruption by the interface and are similar to their bulk values.

5. Bond order analysis

Our bond order analysis of the fcc-oxygen structure further confirms that the interfacial Al_1-O_1 and Al_2-O_1 bonds are very similar to those found in the bulk oxide. For the Al_1-O_1 bond we calculate an average bond order of 0.65 (see Table VI). This is in excellent agreement with the short Al-O bond order of 0.66 found in the interior of the alumina slab. As mentioned earlier, a separate bulk calculation gave a value of 0.67 (Table VI). The three Al_2-O_1 bonds have an average bond order of 0.45. Although this is somewhat smaller than the corresponding bond order of $\simeq 0.5$ in the bulk region of the oxide, this discrepancy can be explained by the slightly longer bond lengths across the interface. In particular, the bond length/bond order values for these three bonds are given by 1.96 Å /0.53, 1.97 Å /0.51, and 2.17 Å / 0.32, respectively. As one can see, the third bond is stretched by 0.2 Å beyond its bulk length of 1.97 Å , and it has a correspondingly smaller bond order, while the other two bonds are in excellent agreement with the bulk values. The close agreement in bond orders between the interfacial Al-O bonds and those found in the bulk oxide clearly demonstrates the ionic nature of the bonding at the fcc-O interface.

The combination of metal-to-oxide charge transfer and the large displacements of the metal atoms results in a local reduction in metallic bonding and a coincident increase in more directional, covalent Al-Al backbonds. (The same be-

havior was seen in the fcc-Al system.) For example, we find a bond order of 0.45 between the Al_2 and Al_3 atoms. In comparison, the normal bond order for an interlayer metallic bond is 0.26. This bond is visible in the $(10\bar{1}0)$ ELF slice from Fig. 11 as the region of high localization just above the interface. There is additional evidence of covalency deeper into the metal slab, where the bond between the Al_3 atom and its neighbor in the subinterface layer is 0.39. Furthermore, the metallic bonds between the Al_1 atom and its nearest-neighbor metal atoms (Al_2, Al_3, and Al_4) are all weaker than in bulk Al: 0.21, 0.19, and 0.21, respectively (see Table VI). This explains the preference for cleavage within the Al (where only weakened metallic bonds must be broken) rather than at the interface (where strong, ionic Al-O bonds form). A similar reduction in Nb metallic bonding was observed in Ref. 17 for the O-terminated Nb/α-Al_2O_3 interface. In contrast to the metal, the bond orders in the oxide slab are virtually undisturbed by formation of the interface; even the bonds in the subinterface layer have bond orders nearly identical to those found in the bulk.

Our finding of ionic bonding supplemented by Al $3sp$–O $2s$ overlap for the fcc-O interface is qualitatively similar to the combination ionic and covalent/metallic bonding found for O-terminated Nb/α-Al_2O_3 in Ref. 17, despite the differences in metallic components. A more thorough study[49] of the adsorption properties of several transition metal overlayers on O-terminated ultrathin Al_2O_3 found that—with the exception of Nb—the preferred method of bonding (at 1 ML coverage) is via metal polarization induced by the oxide's surface Madelung potential.

6. Summary of bonding analysis

Our DOS, ELF, and bond order analyses show that the Al-O bonds formed across the fcc-O interface are very similar to those found in the bulk oxide, and are mainly ionic with a smaller degree of Al $3sp$–O $2s$ overlap. Due to the highly reactive, O–terminated alumina surface, roughly twice as much charge is transferred from the metal to the oxide relative to the fcc-Al system. Finally, although the Mulliken charges and bond orders within the oxide are relatively undisturbed by the presence of the interface, there are significant changes within the metal, where Al-Al covalent backbonds form to compensate for a reduction in metallic bonding and disruption of atomic order near the interface.

VIII. SUMMARY AND CONCLUSIONS

We have conducted an *ab initio* study of the Al(111)/α-Al_2O_3(0001) metal/ceramic interface using bulklike slabs and taking into account the effects of stacking sequence, oxide termination, and full atomic relaxations. A major focus was to determine the nature of the interfacial bonding. We find that, regardless of termination, the optimal interface geometry is obtained for the fcc stacking sequence, which places the metal atoms above the O hole sites in the alumina. An atomic geometry optimization resulted in substantial atomic displacements in the metal near the interface, wherein some atoms were pulled towards the oxide and assume positions which would normally be occupied by the Al^{3+} cations in the bulk crystal. The subsumed atoms are arranged such that they effectively terminate the oxide with a bilayer of Al, *independent* of its initial termination. Based on their positions and electronic structure, it seems more natural to consider these atoms as belonging to the oxide slab rather than to the metal, with the location of the metal-ceramic interface shifted into the metal. These atomic distortions also open up small charge density voids within the near-interface region of the metal, suggesting a possible cleavage point for the interface when placed in a uniform tension field. We examined this possibility by cleaving the interface within the metal and found that separation preferrentially occurs at the original metal/ceramic interface for the fcc-Al geometry. However, the strong bonds at the fcc-O interface favor cleavage within the metal (adhesive metal transfer).

Two methods were used to estimate the ideal work of adhesion. First, we performed a series of total energy versus interfacial separation calculations using unrelaxed slabs and fit the data to the universal binding energy relation to obtain the optimal unrelaxed interfacial separation and adhesion energy. These geometries were then used as starting points for a determination of the relaxed interfacial structures and their corresponding adhesion energies. In allowing for atomic relaxations, we found that both the magnitude and rank ordering of the adhesion energies for the different stacking sequences *changed* relative to the unrelaxed UBER results, underscoring the importance of including these effects. The calculated adhesion energies of 1.36 J/m^2 (LDA) and 1.06 J/m^2 (GGA) for the relaxed fcc-Al interface are in good agreement with the experimental value of 1.13 J/m^2 and suggest that an Al-terminated interface is the most physically realistic structure for low partial pressures of O_2 gas. For the fcc-O interface these values are about an order of magnitude larger, 10.7 J/m^2 and 9.73 J/m^2, respectively.

Finally, we applied several techniques to carefully analyze the interfacial bonding for the optimal fcc-Al and fcc-O structures. Our primary finding is that the interfacial Al-O bonds in both systems are very similar to the cation-anion bonds found in bulk alumina and are therefore mainly ionic with a smaller degree of covalency. In the O-terminated interface this ionic interaction is the dominant bonding mechanism, and it is responsible for the large adhesion energies. However, our ELF and bond order analyses for the fcc-Al interface indicate that there is some additional, covalent bonding between the oxide's surface Al monolayer and the metal. This suggests that the oxide cations could influence the value of W_{ad}. By analyzing the Mulliken charges we determined that there is twice as much charge transfer to the oxide in the O-terminated interface relative to the Al termination and that the charge state of the subsumed atoms is similar to the cation charges found in the bulk oxide. Lastly, the bond orders and Mulliken populations in the oxide are generally unchanged by the presence of the interface, suggesting that most of its bonding requirements are satisfied by oxidizing the subsumed metal atoms. On the other hand, there is a reduction in metallic bonding in the Al near the interface as a result of its distorted atomic structure and

charge transfer to the oxide. This is compensated for by the formation of more directional, covalent-type backbonds.

ACKNOWLEDGMENTS

Computational resources and consulting were provided by the National Computational Science Alliance (NCSA) at the University of Illinois at Urbana-Champaign under Grant No. MCA96N001N. The authors wish to thank J. Hafner for use of the VASP code, P. Ordejón for use of the SIESTA package, D. Sengupta for valuable assistance in implementing the bond order calculation, D. Jennison for a critical reading of the manuscript, and R. Ramprasad and G. Kresse for many useful discussions. Financial support was provided by the National Science Foundation Division of Materials Research under Grant No. DMR9619353. Additionally, D.J.S. gratefully acknowledges the General Motors Corporation for financial support during a summer internship.

*Corresponding author.

†Present address: Sandia National Laboratories, Mail Stop 9161, Livermore, CA 94551. Electronic address: djsiege@sandia.gov

††Present address: GM Research and Development Center, 30500 Mound Rd., P.O. Box 9055, Warren, MI 48090.

⋆http://ceaspub.eas.asu.edu/cms

[1] M. Humenik and W. D. Kingery, J. Am. Ceram. Soc. **37**, 18 (1954).
[2] J. V. Naidich, Prog. Surf. Membr. Sci. **14**, 353 (1981).
[3] J.-G. Li, J. Am. Ceram. Soc. **75**, 3118 (1992).
[4] J. M. Howe, Int. Mater. Rev. **38**, 233 (1993).
[5] M. W. Finnis, J. Phys.: Condens. Matter **8**, 5811 (1996).
[6] J. E. McDonald and J. G. Eberhart, Trans. Metall. Soc. AIME **233**, 512 (1965).
[7] R. G. Barrera and C. B. Duke, Phys. Rev. B **13**, 4477 (1976).
[8] V. Laurent, D. Chatain, C. Chatillon, and N. Eustathopoulos, Acta Metall. **36**, 1797 (1988).
[9] D. Chatain, L. Coudurier, and N. Eustathopoulos, Rev. Phys. Appl. **23**, 1055 (1988).
[10] N. Eustathopoulos, D. Chatain, and L. Coudurier, Mater. Sci. Eng., A **135**, 83 (1991).
[11] P. Hohenberg and W. Kohn, Phys. Rev. **136**, B864 (1964).
[12] W. Kohn and L. J. Sham, Phys. Rev. **140**, A1133 (1965).
[13] M. Kohyama, Modell. Simul. Mater. Sci. Eng. **4**, 397 (1996).
[14] J. Hoekstra and J. Kohyama, Phys. Rev. B **57**, 2334 (1998).
[15] M. Kohyama and J. Hoekstra, Phys. Rev. B **61**, 2672 (2000).
[16] R. Benedek, M. Minkoff, and L. H. Yang, Phys. Rev. B **54**, 7697 (1996).
[17] I. G. Batirev, A. Alavi, M. W. Finnis, and T. Deutsch, Phys. Rev. Lett. **82**, 1510 (1999).
[18] F. Rao, R. Wu, and A. J. Freeman, Phys. Rev. B **51**, 10 052 (1995).
[19] S. Köstlmeier, C. Elsässer, B. Meyer, and M. W. Finnis, in *Microscopic Simulation of Interfacial Phenomena in Solids and Liquids*, edited by P. E. A. Turchi, A. Gonis, and L. Colombo, Mater. Res. Soc. Symp. Proc. No. 492 (Materials Research Society, Pittsburgh, 1998), p. 97.
[20] S. V. Dudiy, J. Hartford, and B. I. Lundqvist, Phys. Rev. Lett. **85**, 1898 (2000).
[21] J. Hartford, Phys. Rev. B **61**, 2221 (2000).
[22] S. Ogata and H. Kitagawa, J. Jpn. Inst. Met. **60**, 1079 (1996).
[23] R. Benedek, A. Alavi, D. N. Seidman, L. H. Yang, D. A. Muller, and C. Woodward, Phys. Rev. Lett. **84**, 3362 (2000).
[24] Y. F. Zhukovskii, E. A. Kotomin, P. W. M. Jacobs, and A. M. Stoneham, Phys. Rev. Lett. **84**, 1256 (2000).
[25] W. Zhang and J. R. Smith, Phys. Rev. Lett. **82**, 3105 (1999).
[26] R. Benedek, D. N. Seidman, M. Minkoff, L. H. Yang, and A. Alavi, Phys. Rev. B **60**, 16 094 (1999).
[27] W. Zhang and J. R. Smith, Phys. Rev. B **61**, 16 883 (2000).
[28] K. Wefers, G. A. Nitowski, and L. F. Weiserman, U.S. Patent No. 5,126,210 (1992).
[29] P. Lamparter and R. Kniep, Physica B **234**, 234 (1997).
[30] K. Wefers and C. Misra (unpublished).
[31] W. Zhang and J. R. Smith, Phys. Rev. Lett. **85**, 3225 (2000).
[32] A. B. Anderson, S. P. Mehandru, and J. L. Smialek, J. Electrochem. Soc. **132**, 1695 (1985).
[33] C. Verdozzi, D. R. Jennison, P. A. Schultz, and M. P. Sears, Phys. Rev. Lett. **82**, 799 (1999).
[34] F. H. Streitz and J. W. Mintmire, Compos. Interfaces **2**, 473 (1994).
[35] F. H. Streitz and J. W. Mintmire, Phys. Rev. B **50**, 11 996 (1994).
[36] J. E. Angelo and M. I. Baskes, Interface Sci. **4**, 47 (1996).
[37] D. L. Medlin, K. F. McCarty, R. Q. Hwang, S. E. Guthrie, and M. I. Baskes, Thin Solid Films **299**, 110 (1997).
[38] M. Vermeersch, R. Sporken, P. Lambin, and R. Caudano, Surf. Sci. **235**, 5 (1990).
[39] M. Vermeersch, F. Malengreau, R. Sporken, and R. Caudano, Surf. Sci. **323**, 175 (1995).
[40] V. E. Puchin, J. D. Gale, A. L. Shluger, E. A. Kotomin, J. Günster, M. Brause, and V. Kempter, Surf. Sci. **370**, 190 (1997).
[41] J. Ahn and J. W. Rabalais, Surf. Sci. **388**, 121 (1997).
[42] P. Guenard *et al.*, Surf. Rev. Lett. **5**, 321 (1997).
[43] J. Toofan and P. R. Watson, Surf. Sci. **401**, 162 (1998).
[44] I. Manassidis, A. D. Vita, and M. J. Gillan, Surf. Sci. Lett. **285**, L517 (1993).
[45] C. Ruberto, Y. Yourdshahyan, and B. I. Lundqvist (unpublished).
[46] P. D. Tepesch and A. A. Quong, Phys. Status Solidi B **217**, 377 (2000).
[47] R. D. Felice and J. E. Northrup, Phys. Rev. B **60**, 16 287 (1999).
[48] X.-G. Wang, A. Chaka, and M. Scheffler, Phys. Rev. Lett. **84**, 3650 (2000).
[49] A. Bogicevic and D. R. Jennison, Phys. Rev. Lett. **82**, 4050 (1999).
[50] D. R. Jennison, C. Verdozzi, P. A. Schultz, and M. P. Sears, Phys. Rev. B **59**, R15 605 (1999).
[51] J. A. Kelber, C. Niu, K. Shepherd, D. R. Jennison, and A. Bogicevic, Surf. Sci. **446**, 76 (2000).
[52] C. Niu, K. Shepherd, D. Martini, J. A. Kelber, D. R. Jennison, and A. Bogicevic, Surf. Sci. **465**, 163 (2000).
[53] D. R. Jennison and A. Bogicevic, Surf. Sci. **464**, 108 (2000).
[54] K. C. Hass, W. F. Schneider, A. Curioni, and W. Andreoni, Science **282**, 265 (1998).
[55] P. J. Eng, T. P. Trainor, G. E. Brown, Jr., G. A. Waychunas, M. Newville, S. R. Sutton, and M. L. Rivers, Science **288**, 1029 (2000).
[56] K. C. Hass, W. F. Schneider, A. Curioni, and W. Andreoni, J.

Phys. Chem. B **104**, 5527 (2000).
[57] L. G. Hector, Jr., G. A. Nitowski, S. M. Opalka, L. Wieserman, D. J. Siegel, H. Yu, and J. B. Adams, Surf. Sci. **494**, 1 (2001).
[58] M. Gautier, G. Renaud, L. P. Van, B. Villette, M. Pollak, N. Thromat, F. Jollet, and J.-P. Duraud, J. Am. Ceram. Soc. **77**, 323 (1994).
[59] J. Bruley, R. Brydson, H. Müllejans, J. Mayer, G. Gutekunst, W. Mader, D. Knauss, and M. Rühle, J. Mater. Res. **9**, 2574 (1994).
[60] G. Kresse and J. Furthmüller, Phys. Rev. B **54**, 11 169 (1996).
[61] A. M. Rappe, K. M. Rabe, E. Kaxiras, and J. D. Joannopoulos, Phys. Rev. B **41**, 1227 (1990).
[62] G. Kresse and J. Hafner, J. Phys.: Condens. Matter **6**, 8245 (1994).
[63] P. Pulay, Chem. Phys. Lett. **73**, 393 (1980).
[64] D. M. Wood and Z. Zunger, J. Phys. A **18**, 1343 (1985).
[65] C. G. Broyden, Math. Comput. **19**, 577 (1965).
[66] D. D. Johnson, Phys. Rev. B **38**, 12 807 (1988).
[67] H. J. Monkhorst and J. D. Pack, Phys. Rev. B **13**, 5188 (1976).
[68] N. D. Mermin, Phys. Rev. **137**, A1441 (1965).
[69] C.-L. Fu and K.-M. Ho, Phys. Rev. B **28**, 5480 (1983).
[70] M. Methfessel and A. T. Paxton, Phys. Rev. B **40**, 3616 (1989).
[71] O. Jepsen and O. K. Andersen, Solid State Commun. **9**, 1763 (1971).
[72] P. E. Blöchl, O. Jepsen, and O. K. Andersen, Phys. Rev. B **49**, 16 223 (1994).
[73] H. Hellmann, *Einfuhrung in die Quantumchemie* (Deuticke, Leipzig, 1937).
[74] R. P. Feynman, Phys. Rev. **56**, 340 (1939).
[75] W. H. Press, S. A. Teukolsky, W. T. Vetterling, and B. P. Flannery, *Numerical Recipes in Fortran 90: The Art of Parallel Scientific Computing*, 2nd ed. (Cambridge University Press, Cambridge, England, 1996).
[76] J. P. Perdew and A. Zunger, Phys. Rev. B **23**, 5048 (1981).
[77] J. P. Perdew *et al.*, Phys. Rev. B **46**, 6671 (1992).
[78] L. Kleinman and D. M. Bylander, Phys. Rev. Lett. **48**, 1425 (1982).
[79] F. D. Murnaghan, Proc. Natl. Acad. Sci. U.S.A. **30**, 244 (1944).
[80] *Thermophysical Properties of Matter*, edited by Y. S. Touloukian, R. K. Kirby, R. E. Taylor, and T. Y. R. Lee (Plenum, New York, 1975), Vol. 12.
[81] C. Kittel, *Introduction to Solid State Physics*, 6th ed. (Wiley, New York, 1986).
[82] G. Simmons and H. Wang, *Single Crystal Elastic Constants and Calculated Aggregate Properties: A Handbook*, 2nd ed. (MIT Press, Cambridge, MA, 1971).
[83] G. N. Kamm and G. A. Alers, J. Appl. Phys. **35**, 327 (1964).
[84] J. Vallin, M. Mongy, K. Salama, and O. Beckman, J. Appl. Phys. **35**, 1825 (1964).
[85] See EPAPS Document No. E-PAPS: PRBMDO-65-019208 for a complete comparision of our bulk and surface properties to those of other recent calculations and experiment. This document may be retrieved via the EPAPS homepage (http://www.aip.org/pubservs/epaps.html) or from ftp.aip.org in the directory /epaps/. See the EPAPS homepage for more information.
[86] *Crystal Structures*, 2nd ed., edited by W. G. Wyckoff (Krieger, Malabar, 1982), Vols. 1–3.
[87] J. C. Boettger, Phys. Rev. B **55**, 750 (1997).
[88] Specifically, these are the ''Al_h'' and standard ''O'' pseudopotentials (pp) from the VASP pp database. We also compared results obtained using ultrasoft pp's for *both* Al and O. These pp's have an undesirable core overlap of nearly 0.4 Å . For this set, we found that the LDA lattice constants were in better agreement with experiment than those given by GGA; however, the LDA bulk modulus was worse (LDA: $a=4.75$ Å, $c=12.94$ Å; $B_0=240$ GPa. GGA: $a=4.82$ Å, $c=13.16$ Å, $B_0=234$ GPa). Although for the bulk these differences are minor, we found that use of ultrasoft pp's for both elements had a significant effect upon our adhesion energies, changing some values by as much as 25%.
[89] P. Richet, J. Xu, and H. K. Mao, Phys. Chem. Miner. **16**, 207 (1988).
[90] *CRC Handbook of Chemistry and Physics*, 67th ed., edited by R. C. Weast (CRC Press, Boca Raton, FL, 1983).
[91] J. C. Boettger, Phys. Rev. B **49**, 16 798 (1994).
[92] V. Fiorentini and M. Methfessel, J. Phys.: Condens. Matter **8**, 6525 (1996).
[93] J. Neugebauer and M. Scheffler, Phys. Rev. B **46**, 16 067 (1992).
[94] J. Schöchlin, K. P. Bohnen, and K. M. Ho, Surf. Sci. **324**, 113 (1995).
[95] R. Ramprasad, D. A. Drabold, and J. B. Adams, in *Mechanisms of Thin Film Evolution*, edited by S. M. Yalisove, C. V. Thompson, and D. J. Eaglesham, Mater. Res. Soc. Symp. Proc. No. 317 (Materials Research Society, Pittsburgh, 1994).
[96] H. B. Nielson and D. L. Adams, J. Phys. C **15**, 615 (1982).
[97] J. R. Noonan and H. L. Davis, J. Vac. Sci. Technol. A **8**, 2671 (1990).
[98] We also calculated these relaxations within the GGA and found that they are essentially identical to the LDA values.
[99] $(2a/3)[10\bar{1}0]_{Al_2O_3(LDA)}=2.722$ Å and $a[\bar{1}10]_{Al(LDA)}=2.808$ Å . The strain rate in our post-GGA calculations is higher (4.9%) since these involved only an evaluation of the total energy using the smaller, fixed LDA lattice constants.
[100] J. Schnitker and D. J. Srolovitz, Modell. Simul. Mater. Sci. Eng. **6**, 153 (1998).
[101] J. R. Smith, T. Hong, and D. J. Srolovitz, Phys. Rev. Lett. **72**, 4021 (1994).
[102] T. Hong, J. R. Smith, and D. J. Srolovitz, J. Adhes. Sci. Technol. **8**, 837 (1994).
[103] T. Hong, J. R. Smith, and D. J. Srolovitz, Acta Metall. Mater. **43**, 2721 (1995).
[104] D. M. Lipkin, J. N. Israelachvili, and D. R. Clarke, Philos. Mag. A **76**, 715 (1997).
[105] D. Chatain, I. Rivollet, and N. Eustathopoulos, J. Chim. Phys. Phys.-Chim. Biol. **83**, 561 (1986).
[106] D. Chatain, I. Rivollet, and N. Eustathopoulos, J. Chim. Phys. Phys.-Chim. Biol. **84**, 201 (1987).
[107] Compare, for example, the LDA and GGA surface energies listed earlier in this paper.
[108] For the Al slab atoms we used an enlarged covalent radius of 1.51Å for the Wigner-Seitz radius (r_{ws}). For the oxide we chose: $r_{ws}^{Al}=1.19$ Å and $r_{ws}^{O}=1.29$ Å , which are scaled averages of the respective covalent and ionic radii. All r_{ws} were scaled so that the sum of the volume of the Wigner-Seitz spheres covered ~100% of the simulation cell volume for the bulk materials.
[109] A. Savin, R. Nesper, S. Wengert, and T. F. Fässler, Angew. Chem. Int. Ed. Engl. **36**, 1808 (1997).

[110] B. Silvi and A. Savin, Nature (London) **371**, 683 (1994).
[111] J. K. Burdett and T. A. McCormick, J. Phys. Chem. A **102**, 6366 (1998).
[112] L. D. Santis and R. Resta, Surf. Sci. **450**, 126 (2000).
[113] R. S. Mulliken, J. Chem. Phys. **23**, 1833, 2343 (1955).
[114] D. Sánchez-Portal, P. Ordejón, E. Artacho, and J. M. Soler, Int. J. Quantum Chem. **65**, 453 (1997).
[115] P. Ordejón, E. Artacho, and J. M. Soler, Phys. Rev. B **53**, 10 441 (1996).
[116] A. M. Stoneham, Appl. Surf. Sci. **14**, 249 (1983).
[117] D. M. Duffy, J. H. Harding, and A. M. Stoneham, Philos. Mag. A **67**, 865 (1993).
[118] M. W. Finnis, Acta Metall. Mater. **40**, S25 (1992).
[119] I. Mayer, Chem. Phys. Lett. **97**, 270 (1983).